Published in final edited form as:
Nat Immunol. 2018 September ; 19(9): 973–985. doi:10.1038/s41590-018-0178-z.

Disruption of an anti-mycobacterial circuit between dendritic and Th cells in human SPPL2a deficiency

Xiao-Fei Kong[1,#], **Ruben Martinez-Barricarte**[1,#], **James Kennedy**[2,*], **Federico Mele**[3,*], **Tomi Lazarov**[4,*], **Elissa K Deenick**[5,6,*], **Cindy S Ma**[5,6,*], **Gaëlle Breton**[7,§], **Kimberly B Lucero**[8,§], **David Langlais**[2,§], **Aziz Bousfiha**[9,10,##], **Caner Aytekin**[11,##], **Janet Markle**[1], **Céline Trouillet**[4], **Fabienne Jabot-Hanin**[12,13], **Cecilia S. Lindestam Arlehamn**[14], **Geetha Rao**[5,6], **Capucine Picard**[13,15,25], **Théo Lasseau**[1], **Daniela Latorre**[3], **Sophie Hambleton**[16], **Caroline Deswarte**[12,13], **Yuval Itan**[1], **Katia Abarca**[17], **Dewton Moraes-Vasconcelos**[18], **Fatima Ailal**[9,10], **Aydan Ikinciogullari**[19], **Figen Dogu**[19], **Ibtihal Benhsaien**[9,10], **Alessandro Sette**[14,20], **Laurent Abel**[1,12,13], **Stéphanie Boisson-Dupuis**[1,12,13], **Bernd Schröder**[21,22,**], **Michel C. Nussenzweig**[7,23,**], **Kang Liu**[8,**], **Frédéric Geissmann**[4,§§], **Stuart G. Tangye**[5,6,§§], **Philippe Gros**[2,§§], **Federica Sallusto**[3,24,§§], **Jacinta Bustamante**[1,12,13,15,###], and **Jean-Laurent Casanova**[1,12,13,23,25,###,@]

[1]St. Giles Laboratory of Human Genetics of Infectious Diseases, Rockefeller Branch, The Rockefeller University, New York City, NY, USA [2]Department of Biochemistry, McGill University, Montreal, QC, Canada [3]Center of Medical Immunology, Institute for Research in Biomedicine, Faculty of Biomedical Sciences, University of Italian Switzerland, Bellinzona, Switzerland [4]Immunology Program, Memorial Sloan Kettering Cancer Center, New York City, NY, USA [5]Immunology Division, Garvan Institute of Medical Research, Darlinghurst, NSW, Australia [6]St Vincent's Clinical School, Faculty of Medicine, UNSW Australia, Darlinghurst, NSW, Australia [7]Laboratory of Molecular Immunology, The Rockefeller University, New York City, NY, USA [8]Department of Microbiology and Immunology, Columbia University Medical Center, New York City, NY, USA [9]Laboratory of Clinical Immunology, Inflammation and Allergy, Faculty of Medicine and Pharmacy of Casablanca, King Hassan II University, Casablanca, Morocco [10]Clinical

[@]Correspondence and requests for materials should be addressed to JLC (jean-laurent.casanova@rockefeller.edu; casanova@rockefeller.edu).
[#,*,§,##,**,§§,###]equal contributions

Data availability

WES data supporting the findings of this study have been deposited in Sequence Read Archive (SRA). Accession numbers: SRP149902. The authors declare that all other data supporting the findings of this paper are available within the paper.

Author contributions

X.-F.K., R.M.-B., J.K., F.M., T. Lazarov, E.K.D., D. Langlais, C.S.M., G.B., T. Lasseau, L.A., C.T., S.B.-D., M.C.N., D. Latorre, J.M., B.S., K.L., G.R., S.G.T., F.G., F.S., P.G., J.B. and J.-L.C. designed experiments. X.-F.K., R.M.-B., F.M., J.K., T. Lasseau, E.K.D., D. Langlais, G.R., C.T., C.S.M., J.M., G.B., J.M., C.T., T. Lazarov, C.D., K.B.L. and D. Latorre conducted experiments. F.J.-H., Y.I. and L.A. performed bioinformatics analysis. X.-F.K, R.M.-B., F.M., J.K., T. Lazarov, E.K.D., D. Langlais, C.S.M., G.B., S.H., L.A., S.B.D., M.C.N., B.S., G.R., S.G.T., F.G., F.S., K.L., P.G., J.B. and J.-L.C. analyzed and/or interpreted data. A.B., C.A., C.P., K.A., D.M.-V., F.A., A.I., F.D. and I.B. provided samples and performed clinical diagnoses and follow-up of the patients. C.S.L.A., A.S. and B.S. contributed critical materials. J.B., J.-L.C. supervised the study. X.-F.K., R.M.-B. and J.-L.C. wrote the manuscript and designed the figures, with contributions from all other authors. All authors edited the manuscript and approved its final version.

Competing financial interests

The authors have no competing financial interests to declare.

Europe PMC Funders Author Manuscripts

Immunology Unit, Department of Pediatric Infectious Diseases, Children's Hospital, CHU Averroes, Casablanca, Morocco [11]Department of Pediatric Immunology, Dr. Sami Ulus Maternity and Children's Health and Diseases Training and Research Hospital, Ankara, Turkey [12]Laboratory of Human Genetics of Infectious Diseases, Necker Branch, INSERM U1163, Necker Hospital for Sick Children, Paris, France [13]Paris Descartes University, Imagine Institute, Paris, France [14]La Jolla Institute for Allergy and Immunology, La Jolla, CA, USA [15]Study Center for Immunodeficiencies, Necker Hospital for Sick Children, AP-HP, Paris, France [16]Primary Immunodeficiency Group, Institute of Cellular Medicine, Newcastle University, Newcastle upon Tyne, UK [17]Department of Pediatric Infectious Diseases and Immunology, Millennium Institute of Immunology and Immunotherapy, School of Medicine, Pontifical Catholic University of Chile, Santiago, Chile [18]Laboratory of Investigation in Dermatology and Immunodeficiencies, University of Sao Paulo Medical School, Brazil [19]Department of Pediatric Immunology and Allergy, Ankara University School of Medicine, Ankara, Turkey [20]University of California San Diego, Department of Medicine, La Jolla, CA [21]Biochemical Institute, Christian Albrechts University of Kiel, Kiel, Germany [22]Institute of Physiological Chemistry, Technical University Dresden, Dresden, Germany [23]Howard Hughes Medical Institute, New York, USA [24]Institute of Microbiology, ETH Zurich, Switzerland [25]Pediatric Hematology and Immunology Unit, Necker Hospital for Sick Children, AP-HP, Paris, France

Abstract

Human inborn errors of IFN-γ immunity underlie mycobacterial diseases. We describe patients with BCG disease who are homozygous for loss-of-function mutations of *SPPL2A*. This gene encodes a transmembrane protease that degrades the N-terminal fragment (NTF) of CD74 (HLA invariant chain) in antigen-presenting cells. CD74 NTF therefore accumulates in the HLA class II^+ myeloid and lymphoid cells of SPPL2a-deficient patients. This toxic fragment selectively depletes IL-12- and IL-23-producing $CD1c^+$ conventional dendritic cells (cDC2s), and their circulating progenitors. Moreover, SPPL2a-deficient memory T_H1^* cells selectively fail to produce IFN-γ when stimulated with mycobacterial antigens in vitro. Finally, *Sppl2a*$^{-/-}$ mice lack cDC2s, have $CD4^+$ T cells that produce small amounts of IFN-γ upon BCG infection, and are highly susceptible to infection with BCG or *Mycobacterium tuberculosis*. These findings suggest that inherited SPPL2a deficiency in humans underlies mycobacterial disease by decreasing the numbers of cDC2s and impairing IFN-γ production by mycobacterium-specific memory T_H1^* cells.

Mendelian susceptibility to mycobacterial disease (MSMD, OMIM# 209950) is characterized by severe clinical disease caused by weakly virulent mycobacteria, such as BCG vaccines and environmental mycobacteria, in otherwise healthy individuals, typically without overt immunological anomalies and with normal resistance to most other infectious agents1,2. These patients are, nevertheless, vulnerable to infections caused by other intramacrophagic pathogens, such as *Salmonella spp.*1,3 and *M. tuberculosis*4 in particular. MSMD can be caused by germline mutations of genes involved primarily in the production of IFN-γ (*IL12B*, *IL12RB1*, *NEMO, ISG15, IRF8, TYK2)*1,5,6 or the response to IFN-γ (*IFNGR1*, *IFNGR2*, *STAT1*, *CYBB)*1,7. Allelic heterogeneity at four of these 10 loci

(*IFNGR1, IFNGR2, STAT1, IL12RB1*) has led to the description of 19 different genetic etiologies of MSMD1. Moreover, at five loci (*STAT1, CYBB, NEMO, TYK2, IRF8*), MSMD is allelic to other clinical conditions associated with a broader range of infections5,8. The discovery that MSMD results from inborn errors of IFN-γ immunity revealed the critical dependence of human anti-mycobacterial immunity on IFN-γ. It also confirmed that IFN-γ acts more as a macrophage-activating factor than as a classical interferon9. Moreover, the identification of MSMD patients with IL-12p40 or IL-12Rβ1 deficiency revealed a critical dependence on IL-12, IL-23, or both, for the production of sufficient levels of anti-mycobacterial IFN-γ1,3,10. However, the genetic basis of this disease has remained elusive in almost half the MSMD patients studied in our laboratory. The cellular basis of MSMD also remains unknown. In particular, it remains unclear which human myeloid and lymphoid cells orchestrate the production of IFN-γ for protective immunity to mycobacteria. In this context, we studied three patients with MSMD of unknown genetic etiology.

Results

Three MSMD patients with homozygous splice mutations of *SPPL2A*

We investigated three patients from two unrelated consanguineous families: a family from Morocco including two affected eight-year-old monozygotic twin sisters (P1 and P2, Kindred A, Fig. 1a)11 and a family from Turkey including an affected 11-year-old boy (P3, Kindred B, Fig. 1a). All three children suffered from BCG disease (see Methods for clinical details). By combining whole-exome sequencing (WES) of P1 and P3 and genome-wide linkage (GWL) for both families, we identified a homozygous essential splice-site mutation in *SPPL2A* (encoding signal peptide peptidase-like 2A, SPPL2a) in each family (Fig. S1a, b, Table S1). There were no other relevant rare, non-synonymous or splice variants of protein-coding genes within the regions linked to MSMD (Table S1). Sanger sequencing confirmed that both P1 and P2 carried a homozygous c.733+1G>A mutation of the splice donor site of *SPPL2A* intron 6, whereas P3 carried a homozygous c.1328-1G>A mutation of the splice acceptor site of *SPPL2A* intron 13 (Fig. 1b, Fig. S1b). The familial segregation of these mutations was consistent with an autosomal recessive (AR) trait (Fig. 1a). These mutations were not found in the gnomAD database (http://gnomad.broadinstitute.org) or our in-house database. The combined annotation dependent deletion (CADD) scores of 27.3 (c. 733+1G>A) and 26.4 (c.1328-1G>A) obtained for these two alleles are well above the mutation significance cut-off (MSC)12 of 2.31 (Fig. 1c, S1c). Both family and population genetic studies, thus, strongly suggested that these three patients from two unrelated kindreds had autosomal recessive (AR) SPPL2a deficiency.

Both *SPPL2A* mutations disrupt splicing of the full-length mRNA

We assessed the functional consequences of these two variants for the splicing of *SPPL2A* mRNAs, by performing RT-PCR on mRNA from Epstein-Barr virus-transformed B (EBV-B) cells of P1, Simian virus 40-transformed fibroblasts (SV40-Fibroblast) from P2, peripheral blood mononuclear cells (PBMCs) of P3, and appropriate healthy controls both WT and heterozygous for the corresponding mutation. We amplified a segment spanning exons 4 to 7 for kindred A and exons 13 to 15 for kindred B. The cells from all patients yielded PCR

products of lower molecular weight (MW) than those obtained for healthy controls, whereas those of heterozygous carriers yielded both products (Fig. 1d). Sanger sequencing of these PCR products showed that the c.733+1G>A (P1 and P2) mutation was associated with the complete skipping of exon 6 in the encoded mRNA, whereas the c.1328-1G>A (P3) mutation was associated with the complete skipping of exon 14 (Fig. 1b). Quantitative PCR showed that cells from the patients expressed about 25-40% the amount of *SPPL2A* mRNA found in healthy controls (Fig. S1d, e). This finding is consistent with nonsense-mediated mRNA decay due to a premature stop codon (Fig. 1e). We then transfected HEK293T cells with plasmids encoding a C-terminally V5-tagged WT protein or mutant *SPPL2A* cDNAs lacking exons 6 or 14 (Δex6 or Δex14, respectively). Immunoblotting with an antibody (Ab) against amino acids 196-210 (a region preserved partially in Δex6 and completely in Δex14 SPPL2a proteins) revealed a protein product with an apparent MW between 76 and 102 kDa for the WT construct (Fig. 1f). We detected no Δex6 SPPL2a protein and a protein of approximately 52 kDa for Δex14 SPPL2a, consistent with the predicted MW of the truncated protein (50 kDa) (Fig. 1F). Immunoblotting with an Ab against the C-terminal V5 tag showed both mutant proteins to be absent. These results indicate that both *SPPL2A* mutations disrupt mRNA splicing and lead to a loss of SPPL2a protein production (for the c. 733+1G>A mutation causing Δex6) or to the production of a truncated protein (the c. 1328-1G>A mutation causing Δex14) in an overexpression system. These findings strongly suggested that the patients had AR complete SPPL2a deficiency.

Accumulation of the N-terminal fragment of CD74 in SPPL2a-deficient cell lines

SPPL2a is an intramembrane protease of the GxGD protease family13. Six proteins, TNF, CD74, FasL, TMEM106B, NRG1, and Bri2, have been identified as possible substrates of this enzyme14–22. A human gene connectome (HGC) analysis of the genes encoding these proteins, taking *IFNG* as the core gene, identified TNF, CD74, and FASL as the only putative substrates significantly related to IFN-γ (http://hgc.rockefeller.edu)23. Germline mutations of the human *FAS* and *FASL* genes underlie autoimmunity without mycobacterial disease24,25. We assessed the impact of SPPL2a deficiency on TNF, a key cytokine for protective immunity against mycobacteria in humans26 (Fig. S1f). The mutations of our patients resulted in the intracellular expression of TNF by a lower percentage of memory $CD4^+$ T cells, but this had no effect on overall TNF secretion *per se* (Fig. S1g, h). Normal amounts of secreted TNF are consistent with both SPPL2a cleaving the TNF NTF after its soluble segment has been released and the redundant function of SPPL2a and SPPL2b in that cleavage15,16. We then considered CD74, the only substrate of SPPL2a to have been confirmed in conditions of constitutive expression19–21,27,28. CD74 is expressed by HLA class II^+ antigen-presenting cells (APC)21. In the endoplasmic reticulum (ER), CD74 forms a heterotrimer with HLA class II α and β chains via the class II invariant chain peptide (CLIP) region. CD74 is transported to the endosomal compartments, where it is processed by four successive proteolytic cleavages, leaving the CLIP fragment associated with the HLA class II molecule and a standalone membrane-bound NTF. In the final step of CD74 processing, SPPL2a mediates the intramembrane cleavage of the NTF (Fig. 2a)19–21. We evaluated the functional consequences of SPPL2a deficiency in patients, by assessing CD74 NTF accumulation in various cell types ex vivo and in cell lines in vitro, with a Ab recognizing the amino acids 12-28 in the N-terminal of human CD74. We found that CD74

NTF levels were much higher in EBV-B cells from P1, IFN-γ stimulated SV40-Fibroblasts from P2, and PBMCs from P3, than in the corresponding cells from healthy donors and *SPPL2A*-heterozygous relatives (Fig. 2b, c). We used a retroviral system to introduce the WT *SPPL2A* allele into EBV-B cells from P1; this rescued the phenotype of CD74 NTF accumulation (Fig. 2c). We also tested all eight *SPPL2A* variants found in the homozygous state in public databases and found that all of these variants rescued CD74 NTF accumulation (Fig. 1c, e, 2d). Moreover, the addition of the inhibitors of SPPL2a function L-685,458 and $(Z\text{-}LL)_2$-ketone, led to the accumulation of CD74 NTF in EBV-B cells from healthy individuals, albeit to a lower extent than in SPPL2a-deficient EBV-B cells (Fig. 2e). No CD74 NTF accumulation was observed with another inhibitor (DAPT) with no inhibitory effects on SPPL2a (Fig. 2e). As previously reported, inhibitors of cathepsin (E64d) stabilized larger intermediates of CD74 degradation (Fig. 2e)29. These results confirmed the complete functional deficiency of SPPL2a, in terms of CD74 NTF cleavage, in the three patients. They also demonstrated that the frequency of SPPL2a deficiency in the general population is well below that of MSMD (about 10^{-5}). Collectively, these findings showed that the two *SPPL2A* mutations underlie AR SPPL2a deficiency in these two kindreds.

Accumulation of CD74 NTF in SPPL2a-deficient leukocytes

We further analyzed the cell type-specific impact of SPPL2a-dependent CD74 NTF accumulation. We first determined by flow cytometry the intracellular CD74 levels in primary monocytes, B, and T cells. We observed that intracellular CD74 staining was stronger in monocytes and B cells from SPPL2a-deficient patients than in those of healthy controls and heterozygous relatives, whereas no such difference was observed for T cells (Fig. 2f, S2a,b). This stronger staining presumably reflects the accumulation of NTF observed on immunoblots of EBV-B cells, PBMCs, and SV40-Fibroblasts (Fig. 2c). We then measure cell surface CD74 expression on these same leukocyte subsets, with an Ab against the extracellular domain of CD74. CD74 expression on the surface of monocytes, B cells, and T cells did not differ significantly between SPPL2a-deficient patients and healthy controls (Fig. 2g, S2a,c). We then identified the leukocyte subsets with the highest amounts of CD74 NTF accumulation, by treating PBMCs from healthy controls with L-685,458, an inhibitor of SPPL2a. The $CD1c^+$ subset of circulating conventional dendritic cells (cDC2s) accumulated the highest amount of CD74 NTF (Fig. 2h, S2d). Circulating $CD141^+Clec9a^+$ conventional DCs (cDC1s), $CD303^+$ plasmacytoid DCs (pDCs), and B cells had intermediate levels of CD74 NTF accumulation following drug treatment, whereas no accumulation was detectable in monocytes, NK and T cells (Fig. 2h, S2d). Thus, in the context of abolished SPPL2a function, CD74 NTF accumulates in various types of human HLA class II^+ APCs, the highest amounts being reached in cDC2s. Moreover, MSMD patients with autosomal dominant (AD) IRF8 deficiency have no cDC2s30.

Human SPPL2a deficiency does not affect B cell immunity

Mice with SPPL2a deficiency have very low B cell counts, low serum IgG_1, IgG_{2a}, IgG_{2b}, IgG_3, IgA and IgM levels, and impaired Ab responses to various antigens19–21. SPPL2a-deficient mice are probably susceptible to pyogenic bacteria31. None of the three patients described here had a B cell deficiency other than slightly lower total IgG levels and, in P1

and P2, slightly higher IgM levels than age-matched controls (Tables S2 and S3). P3 had normal specific Ab titers against vaccine antigens and mounted specific Ab responses following infection with viruses (Table S2). Following inoculation of conjugated pneumococcal vaccines, the three patients mounted normal Ab responses against some, but not all, serotypes of pneumococcal glycans (Table S2). In addition, they had normal proportions of peripheral $CD19^+$ B cells, including transitional, naive, and memory B cells, whereas *Sppl2a*$^{-/-}$ mice displayed a severe B cell deficiency after transitional stage 1 (Fig. S3a,b and Tables S2, S3 and S4). The expression of CD21, IgM, and IgD was normal in the patients' SPPL2a-deficient B cells (data not shown). The percentage of IgG^+ memory B cells was slightly lower in SPPL2a-deficient patients than in age-matched healthy individuals, but the percentage of IgA^+ memory B cells was normal (Fig. S3c). We sorted naive and memory B cells from SPPL2a-deficient patients, heterozygous relatives and healthy controls, and stimulated them with CD40L, together with IL-21. Unlike in *Sppl2a*$^{-/-}$ mice19–21, the secretion of IgM, IgG, and IgA by B cells from patients was similar to that for healthy controls (Fig. S3d). Moreover, unlike B cells from *Sppl2a*$^{-/-}$ mice19–21, the SPPL2a-deficient B cells of the patients had normal surface HLA-DR and BAFF-R expression (Fig. S3e). Finally, the patients displayed none of the pyogenic infections typical of human B cell deficiencies32, providing further evidence of their adequate B cell development, differentiation, and function despite CD74 NTF accumulation. Thus, SPPL2a deficiency in humans seems to differ from the corresponding mouse model in its minimal impact on B cells and humoral immunity in the three children studied.

Human SPPL2a deficiency affects type 2 conventional dendritic cells

Sppl2a$^{-/-}$ mice have a profound deficit of $CD11c^+CD11b^+$ cDCs19–21, which are the equivalent of human $CD1c^+$ cDC2s33. This lack of $CD11c^+CD11b^+$ conventional DCs is CD74-dependent, as CD74 deficiency restores these cells in *Sppl2a*$^{-/-}$ mice19. Three main subsets of DCs are present in human blood: cDC2s, cDC1s, and pDCs34. We analyzed these three circulating DC subsets in controls and SPPL2a-deficient patients. All patients had a significantly lower frequency of $CD1c^+CD11c^{hi}$ HLA-DR^{hi} cDC2s than controls, marginally lower frequencies of $CD141^+Clec9a^+$ cDC1s, but normal frequencies of pDCs (Fig. 3a-I, S4a,b). Total cDC ($CD11c^+$) frequencies were also lower in the patients than in controls (Fig. 3j). These results suggest that humans with AR SPPL2a deficiency have a selective loss of cDC2s. The remaining $CD1c^+$ cells in the patients also displayed elevated HLA-DR expression at the cell surface than controls (Fig. S4c,d), as previously shown in *Sppla2*$^{-/-}$ mice20. CD74 NTF-mediated toxicity probably triggers an unfolded protein response (UPR), thereby inducing endoplasmic reticulum (ER)-stress sensor XBP1 expression, which is an inducer of MHC II expression35. Strikingly, the selective cDC2-deficiency phenotype of these patients resembles that previously observed in the two MSMD patients with AD partial IRF8 deficiency (Fig. 3a-c)30. However, an analysis of cDC1s within the $CD11c^+$ gate, using CD141 and Clec9a Abs, showed that the DC defect of these patients was not restricted to cDC2s. Instead of the two populations seen in healthy controls, the patients had just one $Clec9a^-$ population with abnormally high CD141 expression (Fig. 3d, S4a). The lower frequency of $CD1c^{hi}$ cDC2s observed in both AR SPPL2a-deficient and AD IRF8-deficient patients was not due to low CD1c expression, as the $CD1c^-$ DC population of both healthy controls and SPPL2a or IRF8-deficient patients contained no HLA-$DR^{hi}CD11c^{hi}$

cells, these two markers being characteristics of cDC2s (Fig. S4e). In addition, by contrast to the very high plasma concentrations of Flt3 ligand found in patients with AD GATA2 deficiency and AR IRF8 complete deficiency, who lack multiple types of circulating DC30,36, patients with AD IRF8 and AR SPPL2a deficiency have normal circulating Flt3 ligand (Fig. S4f). As cDC2s are potent producers of IL-12 and IL-2337, we tested the capacity of these patients to produce IL-12p40, a subunit common to these two cytokines38. We stimulated whole blood from healthy controls and SPPL2a-deficient patients with BCG, IFN-γ, or both, and measured IL-12p40 production. We observed no defect of IL-12p40 production in patients with AR SPPL2a deficiency, suggesting that the low frequency of cDC2s in these patients does not cause an overt IL-12 and IL-23 defect in the stimulation conditions used30 (Fig. S4g). Collectively, these data indicated that patients with AR SPPL2a deficiency had a defect of the cDC2 compartment that did not prevent their whole blood from producing IL-12p40 in response to BCG and IFN-γ.

The role of SPPL2a in DC development

We analyzed DC development in the setting of SPPL2a deficiency, by assessing the frequencies of $CD34^+$ progenitors and $HLA\text{-}DR^+$ precursors among the patients' PBMCs. We found normal frequencies of total $CD34^+Lin^-$ progenitors (Fig. S5a), including hematopoietic stem cells/multipotent progenitors (HSC/MPPs), megakaryocyte-erythroid progenitors (MEPs), granulocyte/monocyte progenitors (GMPs), lymphoid-primed multipotent progenitors (LMPPs), multi-lymphoid progenitors (MLPs), and B cell-NK progenitors (BNKPs), and slightly lower frequencies of common myeloid progenitors (CMPs) in the patients than in healthy controls (Fig. 4a, S5a,b). However, the patients had significantly lower frequencies of $CD34^+HLA\text{-}DR^+$ cells (Fig. 4b, S5d,e). Furthermore, among the $Lin(CD3, CD19, CD56, CD14, CD16)^-HLA\text{-}DR^+$ cells, a population including early DC precursors39,40, $CD34^-CD1c^-Clec9a^-CD123^+CD303^+CD141^+CD45RA^{+/int}$ early pre-DCs39 were significantly less frequent in SPPL2a-deficient patients than in healthy controls (Fig. 4c, S5f). This suggests that SPPL2a deficiency impedes DC development at the pre-DC stage, when HLA-DR expression is initiated. We then purified $CD34^+$ cells from healthy donor cord blood and generated DCs in vitro with GM-CSF, SCF, and Flt3 ligand41, with or without the SPPL2a inhibitor L-685,458. SPPL2a inhibition had no effect on the numbers, proportions, or viability of cDC1s, cDC2s, or pDCs on day 6 of differentiation (Fig. 4d,e). However, the increase in intracellular CD74 relative to untreated cells was larger in cDC2s than in the other subsets analyzed, demonstrating that NTF accumulation was due to the inhibition of SPPL2a (Fig. 4f,g). These data suggested that residual SPPL2a activity in the presence of the inhibitor might be sufficient for the development of cDC2s in vitro, but not in patients with the corresponding null genetic defect in vivo. Our data indicated that the chemical inhibition of SPPL2a in peripheral leukocytes from healthy donors ex vivo (Fig. 2e) and during DC differentiation from peripheral stem cells in vitro resulted in the preferential accumulation of CD74 NTF in cDC2. Moreover, the frequency of DC progenitors was low in SPPL2a-deficient patients from the first stages of HLA-II expression, consistent with the role of CD74 in correct HLA-II complex assembly. These findings strongly suggested that the mechanism underlying the paucity of cDC2 cells in SPPL2a-deficient patients involved CD74 NTF toxicity, as proven in the mouse model19,20.

Normal development of CD4+ T helper cells

SPPL2a is expressed strongly in APCs, but only weakly in T cells (Fig. 5a, S2d), suggesting that an intrinsic T cell defect is unlikely in SPPL2a-deficient patients. However, given the very low frequency of circulating cDC2s, we hypothesized that the cytokine production capacity of SPPL2a-deficient $CD4^+$ T helper cells might be impaired due to a defect of the differentiation of naive cells into memory cells in vivo. The three patients had normal counts and proportions of the various circulating T cells subsets: total $CD3^+$, naive and memory $CD4^+$, regulatory T cells, T follicular helper cells and $CD8^+$ naive, central, and effector memory T cells as well as γδ T cells and MAIT cells (Table S3). Moreover, the distribution of the different subsets of memory T_H cells (T_H1, T_H2, T_H17, and T_H1*), as determined by surface phenotype (CCR6, CCR4 and CXCR3), was normal (Fig. 5b,c). Naive and memory $CD4^+$ T cells from healthy individuals and AR SPPL2a-deficient patients were isolated and cultured with T cell activation and expansion (TAE) beads, and cytokine production was measured after five days42. No differences were observed in the production of IFN-γ, IL-4, or IL-17F between memory $CD4^+$ T cells from SPPL2a-deficient individuals and those from healthy donors (Fig. 5d). T_H1 differentiation is IL-12-dependent, whereas T_H17 differentiation is IL-23-dependent43. We then assessed intrinsic defects of $CD4^+$ T cell differentiation due to SPPL2a deficiency, by culturing naive $CD4^+$ T cells in the presence of TAE beads alone (T_H0) or under T_H1, T_H2, or T_H17 polarizing conditions. No impairment in the polarization capacity was observed by measuring the increase in IFN-γ, IL-10, or IL-17F production between naive and polarized T_H cells, suggesting that T_H-cell function is not globally impaired in patients with AR SPPL2a deficiency (Fig. 5e). Given the similarities between AR SPPL2a and AD IRF8 deficiencies, we analyzed $CD4^+$ T cell function in a patient with AD IRF8 deficiency in a similar manner. No impairment of IFN-γ, IL-13, and IL-17A production relative to healthy controls was observed for the patient's $CD4^+$ T cells, suggesting that their polarization capacities were also intact (Fig. 5f). However, when memory $CD4^+$ T cells from this patient were isolated and cultured with TAE beads for five days, the levels of T_H1 cytokines (IFN-γ and TNF), T_H2 cytokines (IL-4, IL-5 and IL-13) and T_H17 cytokines (IL-17A, IL-17F and IL-22) were lower than those for healthy control cells, suggesting that AD IRF8 deficiency impairs the maintenance of the $CD4^+$ T cell-mediated memory response or that these cells undergo limited differentiation in vivo (Fig. 5g). In conclusion, SPPL2a deficiency does not seem to result in any major $CD4^+$ T cell phenotype as measured ex vivo, whereas AD IRF8 deficiency causes a broad defect of the $CD4^+$ memory T cell compartment.

Impaired production of IFN-γ by mycobacterium-specific memory CD4+ T cells

We investigated subtler defects of T cell responses to mycobacteria, by isolating two subsets of memory $CD4^+$ T cells from healthy controls and patients with AR SPPL2a or AD IRF8 deficiency, as determined on the basis of CCR6 expression44. The polyclonal $CD4^+CCR6^+$ (comprising T_H17 and T_H1*) and $CD4^+CCR6^-$ (comprising T_H1 and T_H2) memory T cell populations were initially expanded by incubation with IL-2 and phytohemagglutinin (PHA)45. The $CD4^+CCR6^+$ and $CD4^+CCR6^-$ polyclonal T cell lines from patients and controls displayed the same frequencies of IFN-γ^+ cells upon stimulation with PMA plus ionomycin and produced equal amounts of IFN-γ upon activation with PMA and ionomycin, or anti-CD3/28 Abs (Fig. S6a-f). The T cell lines were then analyzed for

reactivity to viral, bacterial, and fungal antigens presented by autologous irradiated B cells, as measured by [^{3}H]-thymidine incorporation. The frequencies of CD4$^+$CCR6$^+$ T cells reacting with antigens from BCG or *M. tuberculosis* (MTB) were similar in healthy controls and patients with SPPL2a deficiency (Fig. 6a). By contrast, BCG- or MTB-specific cells were less frequent or absent in patients with AD IRF8 deficiency (Fig. 6a). SPPL2a-deficient patients had a high frequency of CD4$^+$CCR6$^-$ T cells against viral antigens (CMV, EBV, Flu, RSV), whereas the frequency of these cells was variable in healthy donors and IRF8-deficient patients, possibly reflecting differences in exposure or vaccination (Fig. S6g). Notably, in patients with SPPL2a deficiency, IFN-γ production was much weaker in CD4$^+$ CCR6$^+$ T cells responding to BCG or MTB antigens (Fig. 6b,c), whereas IFN-γ production by T cells responding to viral antigens was similar to that of healthy donors (Fig. 6d). The IFN-γ production defect was also observed in BCG-responding CD4$^+$CCR6$^-$ cells (Fig. S6h,i). These data suggested that SPPL2a-deficient patients displayed a mycobacterium-specific IFN-γ production defect by memory CD4$^+$ T cells. We confirmed that the responding T cell lines were actually T_H1* cells expressing the characteristic CCR4, CXCR3, and CCR6 markers (Fig. S6j). The few mycobacterium-specific CD4$^+$CCR6$^+$ T cells from patients with AD IRF8 deficiency also displayed low IFN-γ production (Fig. 6b,c). IRF8-mutated virus-specific CD4$^+$CCR6$^-$ T cells also displayed weak IFN-γ production, suggesting a broader defect of memory T cells in these patients than in SPPL2a-deficient patients (Fig. 6d). This is consistent with the study of ex vivo cytokine production by CD4$^+$ memory T cells described above. The strong accumulation of CD74 NTF in the B cells used might affect their capacity to act as APCs. We thus pulsed EBV-B cells from P1, non-transduced or transduced with a retrovirus generated with an empty vector or a wild-type *SPPL2A* cDNA, with MTB peptides (which do not require processing) or whole MTB antigens (which require processing), using them as APCs to stimulate MTB-specific T cell clones from P1 and P2. There were no differences in the proliferation of T cells, suggesting that the capacity of the patients' B cells to take up whole antigens and to present the processed peptides is intact (Fig. S6k). Similar results were obtained when Flu vaccine was used to stimulate Flu-specific T cell clones (Fig. S6k). Collectively, these data showed that SPPL2a-deficient patients displayed a narrow immunological phenotype, with abnormally small numbers of cDC2s and poor IFN-γ production by mycobacterium-specific T_H1* cells. On the contrary, IRF8-mutated patients displayed a broader immunological phenotype, but with two features in common with that of SPPL2a-deficient patients: small numbers of cDC2s and impaired IFN-γ production by mycobacterium-specific T_H1* cells.

IRF8 controls *SPPL2A* expression

Given the phenotypic similarities between AR SPPL2a and AD IRF8 deficiencies we hypothesized that there might be a physiological connection between SPPL2a and IRF8. We investigated whether murine IRF8 exerted transcriptional control over *Sppl2a* expression. We performed ChIP-Seq analyses on mouse bone marrow-derived macrophages (BMDM) and peritoneal macrophages. We found binding sites for STAT1, IRF1 and IRF8 in the *Sppl2a* promoter, suggesting that the expression of mouse *Sppl2a* is under the control of these transcription factors (Fig. S7a)46,47. We analyzed EBV-B cells from healthy controls, and patients with AR complete STAT1, IRF8, and SPPL2a deficiencies. We found that SPPL2a expression was slightly weaker than normal in EBV-B cells lacking functional

IRF8, consistent with the ChIP-Seq data obtained for mice (Fig. S7b). We also analyzed the SPPL2a expression of total lymphocytes, B cells and T cells from two patients with AD IRF8 deficiency. We found no differences between these patients and healthy controls, consistent with both the partial nature of AD IRF8 deficiency and the expression of IRF8 predominantly in cDC1s and cDC2s, two subsets lacking in these patients (Fig. S7c,d). Our data show that mouse IRF8 binds to the *Sppl2a* promoter, suggesting that the human ortholog may control *SPPL2A* transcription.

Sppl2a$^{-/-}$ mice are susceptible to mycobacterial infection

We investigated the role of mouse SPPL2a in protective immunity to mycobacteria in vivo, by infecting wild-type and *Sppl2a*$^{-/-}$ mice with live BCG. *Sppl2a*$^{-/-}$ mice have low frequencies of CD11c^{+}CD11b^{+} cDC2s (Fig. 7a, S7e). *Sppl2a*$^{-/-}$ mice developed significantly greater splenomegaly than wild-type mice three and six weeks after infection, and significantly higher BCG colony-forming unit (CFU) counts were obtained six weeks post-infection, indicating greater susceptibility to BCG infection (Fig. 7b,c). Both the size of the IFN-γ^{+} CD4^{+} and CD8^{+} T cell fraction and the production of IFN-γ by splenocytes (after stimulation with BCG or PMA-ionomycin) at three and six weeks post-infection were much lower in *Sppl2a*$^{-/-}$ mice than in wild-type controls (Fig. 7d). *Sppl2a*$^{-/-}$ CD4^{+} and CD8^{+} T cells also produced less TNF than WT cells (Fig. 7e). Mouse CD4^{+} T cells mount a classical T_H1 response to mycobacterial infection, different from the T_H1* response observed in humans. We cannot therefore conclude that the impairment of IFN-γ production in mice is due to T_H1* cells. Nevertheless, these experiments show that mouse SPPL2a is required for optimal IFN-γ production by T cells upon mycobacterial infection. We also infected *Sppl2a*$^{-/-}$ and wild-type mice with a MTB aerosol. At 200 days post-infection, all wild-type mice were still alive, whereas all the *Sppl2a*$^{-/-}$ mice were dead (Fig. 7f). Mice infected with a MTB aerosol had higher lung MTB CFU counts 60 days after infection (Fig. 7g). The total number of cells in the lungs and the numbers of CD4^{+} T cells, CD8^{+} T cells, CD11b^{+}Ly6C^{+} monocytes, and CD11b^{+}F4/80^{+} macrophages were higher than those of wild-type mice 60 days after infection, and the numbers of neutrophils and CD11b^{+}Ly6C^{+} monocytes were already higher than those in wild-type mice 30 days after infection (Fig. 5h-m, S7e). *Sppl2a*$^{-/-}$ mice produced larger amounts of IFN-γ, TNF, and IL-12p40 than wild-type mice, as shown by analyses of lung homogenates, consistent with the higher leukocyte infiltration into the lungs in these mice (Fig. 7n). Thus *Sppl2a*$^{-/-}$ mice lack CD11b^{+}CD11c^{+} cDCs (cDC2), are susceptible to both BCG and MTB infections in vivo, and their T cells produce low IFN-γ upon mycobacterial infection in vivo.

Discussion

We describe here AR complete SPPL2a deficiency, as a genetic etiology of MSMD. We also show that *Sppl2a*$^{-/-}$ mice are susceptible to BCG and MTB. Impaired SPPL2a activity, whether genetic or pharmacological in origin, causes CD74 NTF to accumulate in H-2 and HLA class II^{+} APCs in mice and humans, respectively. This accumulation leads to a profound B cell deficiency in *Sppl2a*$^{-/-}$ mice19–21 but not in SPPL2a-deficient humans. By contrast, both mice and humans with SPPL2a deficiency have a profound defect of the cDC2 compartment. This myeloid phenotype is due to CD74 NTF accumulation, as NTF levels in

cDC2s are highest after the pharmacological inhibition of SPPL2a in healthy donor cells. Moreover, circulating pre-DC progenitors have a low abundance in SPPL2a-deficient patients, from the first stage of HLA-class II expression. Finally, the cDC2 deficiency is rescued in vivo by the genetic ablation of CD74 in *Sppl2a*$^{-/-}$ mice19–21. A complete lack of the three main circulating DC subsets (cDC1s, cDC2s, and pDCs) has been observed in patients with AD GATA2 or AR IRF8 deficiency, both of which cause mycobacterial disease and other infections30,48. AD IRF8 deficiency, a genetic etiology of MSMD, was thought to cause an isolated defect of circulating CD1c^{+} cDC2 cells30. However, our present, detailed analysis revealed that both types of conventional DCs — cDC1s and cDC2s — are actually affected in these patients. By contrast, AR SPPL2a deficiency results in an isolated cDC2 defect, highlighting the crucial role of this human DC population in anti-mycobacterial immunity.

We also found that patients with AR SPPL2a deficiency have a profound defect of mycobacterium-specific IFN-γ production by the CD4^{+} memory T cells of the T_H1* subset. Paradoxically, T_H1* cell counts were normal in the blood of these patients, and these cells proliferated normally in response to mycobacterial antigens, and produced IFN-γ upon polyclonal mitogenic stimulation in vitro. Moreover, our study shows that patients with AD IRF8 deficiency also have a more severe memory CD4^{+} T cell defect, with poor proliferation of T_H1* cells in response to mycobacterial antigens in vitro. Nevertheless, the clinical phenotype of MSMD is identical in patients with these two deficiencies. Despite some immunological differences between AR SPPL2a-deficient patients and AD IRF8-deficient patients, these two genetic diseases share three core phenotypes: a defect of cDC2, a defect of mycobacterium-specific T_H1* cells, and a clinical phenotype of MSMD. These findings suggest that cDC2 and T_H1* cells play an essential role in human anti-mycobacterial immunity. The link between these two disorders is highlighted by the observation that transcription of the mouse *Sppl2a* gene is controlled by various transcription factors including IRF8. We also found that SPPL2a levels were slightly lower than normal in EBV-B cells with complete IRF8 deficiency. IRF8 is probably more critical for the expression of SPPL2a in DCs. However, these cells are lacking in patients with either AR or AD IRF8 deficiency, making it impossible to assess SPPL2a expression in IRF8-deficient myeloid cells.

Our findings suggest that cDC2s may be the key cells presenting mycobacterial peptide antigens to CD4^{+} T cells. The cDC2 deficiency in patients with AR SPPL2a deficiency might cause defective priming in mycobacterium-specific T_H1* cells. The normally high IL-12 and IL-23 production by cDC2 cells are probably relevant37. Indeed, AR deficiencies of IL-12p40 or IL-12Rβ1 underlie MSMD1,3,10. Defective IL-12 and IL-23 stimulation in the course of T cell priming might prevent the correct development of T_H1* cells in patients with AR SPPL2a deficiency. Overall, our findings suggest that cDC2s are required in vivo for T_H1* priming following the presentation of mycobacterial antigens. There is probably a causal relationship between the global cDC2 and narrow T_H1* phenotypes in these patients, given the multiple known relationships between the cells involved (DC and T_H) and their relevant products (IL-12, IL-23 and IFN-γ). The myeloid and lymphoid phenotypes are both broader in patients with IRF8 deficiency than in those with SPPL2a deficiency, providing further support for a connection. The core myeloid phenotype, with a global cDC2/IL-12-23

defect, or the core lymphoid phenotype, with a mycobacterium-specific T_H1*/IFN-γ defect, or both, might also cause a clinical phenotype of MSMD in other patients1,3,10. It is also possible that SPPL2a is required for the proper expression of other anti-mycobacterial molecules49,50. Further genetic and immunological studies of patients with unexplained MSMD are required to delineate more accurately the molecular and cellular basis of protective immunity to mycobacteria in humans.

Online Methods

Patients and clinical information

Two of the patients studied (P1 and P2) are twins born in 2009 to first-cousin Moroccan parents. They were vaccinated with BCG at birth and presented with unilaterally enlarged and inflammatory axillary lymph nodes at nine months of age. The enlarged lymph nodes were surgically removed. Biopsy confirmed the presence of acid-fast bacilli (AFB), consistent with mycobacterial infection. P1 and P2 had normal counts of neutrophils, monocytes, $CD19^+$ B cells, $CD3^+$, $CD4^+$, $CD8^+$ T cells and NK cells. No immunoglobulin, respiratory burst or complement defects were found (Supplementary Table 3). No complications had been observed during the pregnancy, but neonatal asphyxiation was noted during the delivery. MSMD was subsequently diagnosed. Neither of the patients presented any other episodes of mycobacterial infection by the time of clinical evaluation at three years of age. In addition to MSMD, the patients displayed hereditary spastic paraplegia due to a homozygous p.R1105X mutation of the *AP4E1* gene11.

P3 is a boy born to first-degree consanguineous parents in Turkey in 2007. He presented with a two-month history of left axillary lymphadenopathy. He was vaccinated with BCG, on the left shoulder, at the age of two months. At the age of six months, he was treated with isoniazid after a positive tuberculin skin test (TST) (22 x 22 mm), possibly due to contact with his aunt, who had active pulmonary TB. He had a normal thoracic computed tomography scan at the time. His parents and brother are healthy. His aunt, grandfather, great uncle and great aunt had suffered from pulmonary TB. Physical examination was unremarkable, with the exception of an enlarged lymph node (3x3 cm) in the left axillary region. Leukocyte count, absolute neutrophil count and absolute lymphocyte count were normal. Serum IgG level was low (Table S2), whereas serum IgA, IgM and IgE levels were normal for age. Peripheral blood lymphocyte subsets were normal. Neutrophil function in the neutrophil oxidative burst assay (DHR) was normal. CD212 (IL-12Rβ1) expression was normal (CD212: 83%, control: >80%) on the surface of activated T cells. The tuberculin skin test (TST) was positive (10×10 mm). The enlarged axillary lymph node was excised and dissected. Large amounts of calcified material were drained from the lymph node during dissection. Histological examination revealed a necrotizing granulomatous inflammation. Ziehl-Neelsen staining revealed the presence of AFB. MTB complex PCR and culture were negative. MSMD was diagnosed and anti-mycobacterial tritherapy was initiated. P3 is now 11 years old and remains free from mycobacterial disease and other infectious diseases.

Ethics statement

The study was approved and performed in accordance with the institutional ethics committee of Necker-Enfants Malades Hospital, Paris, France and the Rockefeller University Hospital, New York, USA. Informed consent was obtained for all the patients and healthy control volunteers reported in the study.

Cell culture and cell isolation

HEK293T cells and SV40 fibroblasts were cultured in DMEM (Gibco) supplemented with 10% FCS. Phoenix A retroviral packaging cells were cultured in IMDM (Gibco) supplemented with 10% FCS. EBV-B cells were cultured in RPMI (Gibco) supplemented with 10% FCS. PBMCs were isolated by Ficoll-Paque™ PLUS (GE Healthcare) centrifugation and cultured in RPMI (Gibco) supplemented with 10% FBS. All cell lines used were tested for mycoplasma and were negative. HEK293T and Phoenix A cells were purchased from ATCC. B cells and fibroblasts from healthy controls or patients were immortalized in house with EBV or SV40 virus respectively. None of the cells described above have been authenticated but the genotypes at the site of the mutations studied in this report have been confirmed

SPPL2a overexpression

A WT *SPPL2A* plasmid was purchased from Origene and *SPPL2A* was excised and inserted into a pcDNA3.1-V5 (Invitrogen) or pLZRSiresΔNGFR (Addgene) plasmid. pLZRSiresΔNGFR, containing WT *SPPL2A*, the mutants studied in this report (Δex6 and Δex14) or the variants described in genomAD (http://gnomad.broadinstitute.org) were used to transfect Phoenix A cells, retroviruses were produced and used to transduce EBV-B cells from P1, as previously described51. HEK293T cells were transfected in the presence of Lipofectamine LTX reagent (Invitrogen), with pcDNA3.1-V5 containing WT *SPPL2A* or the mutant cDNAs studied here.

SPPL2a inhibition in EBV-Bs or PBMCs

Freshly isolated PBMCs or EBV-B cells (10^6 cells/ml) in RPMI supplemented with 10% FCS were incubated with or without 1 μM DMSO, 1 μM gamma secretase/SPPL inhibitor L-685,458 (EMD Millipore), 10 μM $(Z\text{-}LL)_2$ ketone (Santa Cruz), 10 μM calpain activation inhibitor E64d (Santa Cruz) or 10 μM DAPT (another gamma secretase inhibitor, from R&D Systems) for 5 h for cytokine production and for 24 hours to study CD74 accumulation at 37°C, to mimic the conditions of SPPL2a deficiency.

Immunoblotting

Proteins were extracted with whole-cell lysate buffer containing 20 mM Tris-HCl pH 7.4, 140 mM NaCl, 2 mM EDTA, 50 mM NaF, 1% NP40 supplemented with protease inhibitor cocktail (Complete mini, Roche); proteins were quantified with the Bradford assay. Lysates (50 μg of protein) were mixed with Laemmli loading buffer and incubated at 55°C for 5 minutes before being subjected to electrophoresis in a 4-12% acrylamide precast SDS-PAGE gel (BioRad). The following Abs were used for immunoblotting: rabbit anti-human SPPL2a C-term52, rabbit anti-human SPPL2a epitope 8 (“ENLKAVTTEDREMRK”, residues

196-210 of human SPPL2a, provided by Dr. Bernd Schröder), anti-CD74 (ab97479, Abcam), anti-GAPDH HRP (sc-25778, Santa Cruz) and anti-V5-HRP (R96125, Invitrogen) Abs.

ELISA for human cytokines

Flt3 ligand, TNF and IL-12p40 levels were determined by ELISA, with commercial kits, according to the manufacturer's instructions (R&D Systems).

Flow cytometry and Imagestream

Intracellular CD74, IRF8 and SPPL2a levels were determined in various subsets of PBMCs, by first distinguishing between live and dead cells with LIVE/DEAD fixable aqua (Life Technologies) and then staining for surface markers with anti-CD4 APC/Cy7 (RPA-T4, 300518, BioLegend), anti-CD8 V450 (RPA-T8, 560347, BD), anti-CD45RO Percp/Cy5.5 (UCHL1, 560607, BD Biosciences), anti-CCR7 PE/Cy7 (G043H7, 353226, BioLegend), anti-CD16 APC/Cy7 (3G8, 302016, BioLegend), anti-CD20 PE (2H7, 555623, BD Biosciences), anti-CD56 A700 (B159, 557919, BD Biosciences), anti-HLA-DR Pacific blue (L243, 307624, BioLegend), anti-CD11c Percp/Cy5.5 (BU15, 307624, BioLegend), anti-CD1c APC/Cy7 (L161, 331520, BioLegend), anti-CD141 PE (M80, 344104, BioLegend), anti-CD123 PE/cy7 (6H6, 30601, BioLegend), and anti-CD268 (BAFF-R, 11C1, BioLegend) Abs, at a dilution of 1/50. Cells were then fixed and permeabilized with BD Cytofix/Cytoperm plus (BD Biosciences), according to the manufacturer's instructions. Intracellular proteins then were stained by incubation with anti-SPPL2a C-term (1/1000) or anti-SPPL2a epitope 8 (1/1000), anti-IRF8 (sc-6058, Santa Cruz) (goat), anti-STAT1 (rabbit) (sc-345, Santa Cruz) or anti-CD74 (ab22603, Abcam) (Pin.1, 1/500) Abs for 45 minutes at room temperature, in PBS supplemented with 5% BSA and 0.1% saponin, and then for 45 minutes with goat anti-rabbit Alexa488 (1/1000) (Invitrogen) or donkey anti-goat Alexa 488 (Invitrogen) in PBS supplemented with 5% BSA and 0.1% saponin. Cells were then processed on an Image Stream-X or BD LSR-II machine. Intra- and extracellular CD74 levels in the monocytes, B cells and T cells of controls and patients were assessed by surface staining with anti-CD20 FITC (347673, BD, Clone L27), anti-CD3 BV421 (562426, BD, UCHT1) and anti-surface CD74 (326807, Biologend, LN2) (if sCD74 was to be assessed) Abs, followed by fixation in 2% formaldehyde, and washing with PBS supplemented with 0.1% BSA and 0.5% saponin. Anti-intracellular CD74 Ab (Abcam) in PBS supplemented with 0.1% BSA and 0.5% saponin was then added. Lymphocytes and monocytes were gated individually on the basis of their SSC and FSC properties. $CD3^+$ were considered to correspond to T cells, and $CD20^+$ cells were identified as T cells.

DC immunophenotyping was performed on cryopreserved cells after thawing by adding 1 ml FBS at 37°C to cryopreservation tubes containing 1 ml frozen PBMCs. The thawed mixture was transferred to a 15 ml conical tube and 13 ml of PBS, 0.5% BSA, 2 mM EDTA at room temperature was added. The tubes were centrifuged at 300 x *g* for 7 minutes at 4°C. The supernatant was discarded and the cells were resuspended in 10 ml PBS, 0.5% BSA, 2 mM EDTA at 4°C and placed on ice. Cell numbers and viability were assessed by trypan blue staining in a counting chamber. $1x10^6$-$1x10^7$ cells were transferred to a 5 ml round-bottomed polystyrene tube for staining. The tubes were centrifuged at 300 x *g* for 7 minutes

Europe PMC Funders Author Manuscripts

at 4°C and the supernatant was discarded. The cells were resuspended at a density of ≤1x10^7 cells per 20 μl and FcR blocking reagent (Miltenyi Biotec: 130-059-901) was added at a 1/10 dilution. The tubes were vortexed to resuspend the cells and left on ice for 15 minutes before staining. The samples were stained with anti-CD1c (BDCA-1) FITC (AD5-8E7, Miltenyi: 130-090-507), anti-CD3 PE (UCHT1, mouse IgG1, Beckman Coulter: A07747), anti-CD15 PE (VIMC6, mouse IgM, Miltenyi Biotec: 130-091-375), anti-CD19 PE (HIB19, mouse IgG1 κ, eBioscience: 12-0199-73), anti-CD56 PE (MY31, mouse IgG1 κ, BD Biosciences: 345810), anti-NKp46 PE (BAB281, mouse IgG1, Beckman Coulter: PN IM3711), anti-HLA DR PerCP (L243 (G46-6), muIgG2a k, BD Biosciences: 347402), anti-CD16 PE/Cy7 (3G8, mouse IgG1, BD Biosciences: 557744), anti-CD11c APC (S-HCL-3, Mouse IgG2b k, BD Biosciences: 333144), anti-CD141 (BDCA-3) Abs, VioBlue (AD5-14H12, Miltenyi Biotec: 130-097-325), anti-CLEC9a VioBlue (8F9, Miltenyi Biotec: 130-099-906) and anti-CD14 APC Alexa750 (M5E2, BioLegend, 301820) Abs. All Abs were used at a dilution of 1/100, except CD303 and HLA-DR, which were used at a dilution of 1/50, with ≤1x10^7cells/50 μl. The cells were stained away from direct light for 30 minutes at 4°C. They were then washed in 1 ml of 0.5% BSA in PBS at 4°C; 2 mM EDTA was added and the cells were centrifuged at 300 x *g* for 7 minutes at 4°C. The supernatant was discarded. The cells were resuspended in 200 μl of 0.5% BSA, 2 mM EDTA in PBS at 4°C, and placed in the dark until their use for flow cytometry. The samples were analyzed on an Aria II flow cytometer, and Three star FlowJo v9 was used for data analysis.

Progenitor immunophenotyping: Classical FSC/SSC gates and zombie yellow viability stain were used to define live cells. Doublets were removed based on FSC-A/FSC-W. From live single cells, hematopoietic progenitors were identified as $CD34^+$ Lin(CD3, CD14, CD16, CD19, CD56, CD66b, CD11c, $CD303)^-$. The progenitor populations studied were further defined by the following gating strategies: HSC/MPPs ($CD38^-CD45RA^-CD10^-$), MLP ($CD38^-CD45RA^+CD10^+$), LMPP ($CD38^-CD45RA^+CD10^-$), BNKP ($CD38^+CD45RA^+CD10^+$), CMP ($CD38^+$ $CD10^-$ $CD45RA^-CD123^{int}$), GMP ($CD38^+$ $CD10^-$ $CD45RA^+CD123^{int/hi}$), MEP ($CD38^+$ $CD10^-$ $CD45RA^-CD123^{lo}$).

Early pre-DC identification: Classical FSC/SSC gates and zombie yellow viability stain were used to define live cells. Doublets were removed based on FSC-A/FSC-W. $CD14^+$, $CD14^+/CD16^+$, and $CD16^+$ monocytes were excluded from the live single cells. From the non-monocyte population, $Lin(CD3/19/56)^-$ $HLA\text{-}DR^+$ cells were gated. We excluded cDC2s and cDC1s from Lin-$HLA\text{-}DR^+$ cells on the basis of CD1c and Clec9a expression, respectively. Pre-DCs were then identified from the remaining fraction as Lin-$HLA\text{-}DR^+CD34^-CD1c^-Clec9a^-CD123^+CD303^+CD141^+CD45RA^+$/int.

PCR and qPCR primers and probes

mRNA was extracted with the RNeasy Mini Kit (Qiagen) and treated with DNase (Roche) before reverse transcription. A probe spanning exons 2 and 3 of *SPPL2A* was used for qPCR on the resulting cDNA (Hs00607726_mH, Thermo Fisher Scientific), and 18S (Hs99999901_s1, Thermo Fisher Scientific) or *GUS* (4310888E, Thermo Fisher Scientific) probes were used for normalization. The following primers were used to amplify the region containing exon 6 or exon 14 of the cDNA: cSPPL2A 4F: TGTATTCTCCATCGTGGCCT,

cSPPL2A 7R: ACATGCAATCGTGCATTGTCC; cSPPL2A 13F ACCAGGCCTGTTGATTGCAT; cSPPL2A 15R: GCTGGACAATCTGTTCACCA. For amplification and Sanger sequencing of the genomic DNA region containing the mutation, we used the following primers: gSPPL2A 6F: CAGATCATCTCTGGAGAGTAGCA; gSPPL2A 6R: TCAGAGTAACAGAGACCTAACACT; gSPPL2A 14F TGAAATGACTAACCAGTTTCCACA; gSPPL2A 14 R: GCAGGGGAGGTCACAAATGA.

WES and identification of the mutations

WES was performed by the New York Genome Center, with an Illumina HiSeq 2500 machine, and the Agilent 71 Mb SureSelect exome kit, in accordance with the manufacturer's instructions. BWA (v.0.7.12)53 was used to align the reads with the human reference genome hg19, before recalibration and annotation with GATK (v.3.4-46)54, PICARD (http://picard.sourceforge.net/) (v.1.92) and ANNOVAR (v.07142014)55. Further filtering of the variants was achieved with our own in-house software.

For the genome-wide linkage analysis, all members of the two families were genotyped with the Affymetrix Genome-wide Human Mapping 250K chip, with genotype calling with the Affymetrix Power Tools Software Package (http://www.affymetrix.com/estore/partners_programs/programs/developer/tools/powertools.aff). SNPs presenting more than one Mendelian inconsistency were discarded. SNPs were further filtered with population-based filters, using PLINK software56, according to the ethnicity of the kindred. We then used 163807 autosomal SNP markers for parametric multipoint linkage analyses with MERLIN57 considering founders to be second-degree relatives, assuming autosomal recessive inheritance with complete penetrance, and a damaging allele frequency of 10^{-4}. The family founders and unrelated individuals from HapMap CEU were used to estimate allele frequencies for the two kindreds, and to define linkage clusters, with an r^2 threshold of 0.4.

cDC2 in vitro differentiation assays

Human cord blood (CB) units were purchased from the New York Blood Center. Blood was subjected to density centrifugation on Ficoll-Paque, and granulocyte, monocyte and dendritic cell progenitors (GMDPs) were isolated from mononuclear CB cells. These progenitor cells were then cultured on MS-5 cell strom plus cytokines (Flt3LG, SCF and GM-CSF) with or without SPPL2a inhibitor (1 μM; gamma secretase inhibitor L-685,458 (EMD Millipore)), 1 μM DMSO or 10 μM DAPT. SPPL2A inhibitor, DAPT and DMSO were added daily to the culture. Cells were harvested on day 6, for flow cytometry analysis of the culture output and intracellular CD74 expression (mouse anti-human CD74 Ab, Biolegend). For a more detailed protocol, see 58.

B and T cell phenotyping

T cells: PBMCs were incubated with the following mAbs anti-CD4 (563028, SK3, BD) BV711, anti-CD45RA (11-0458-41, HI100, eBioscience) FITC, anti-CD127 (351309, AO19D5, Biolegend) BV421, anti-CD25 (564033, 2A3, BD) PE-Cy7, anti-CXCR5 (558113, RF8B2), BD) A647, anti-CXCR3 (353713, Go25H7, BioLegend) PerCP-Cy5.5

and anti-CCR6 (559562, 11A9, BD) PE and the proportions of regulatory T cells ($CD4^+CD127^{lo}CD25^{hi}$), total memory ($CD4^+CD45RA^-$), and cTfh ($CD4^+CD45RA^-CXCR5^+$) cells were determined. B cells: PBMCs were incubated with the following mAbs anti-CD20 (347673, L27, BD) FITC, anti-CD19 (563036, SJ25C1, BD) BV711, anti-CD27 (555441, M-T271, BD) PE-Cy7, anti-CD10 (340923, HI10a, BD) APC, and the frequencies of transitional ($CD20^+CD27^-CD10^+$), naive ($CD20^+CD27^-CD10^-$), and memory ($CD20^+CD27^+CD10^-$) B cells were determined. Cells were also stained with anti-IgG (563246, G18-145, BD) BV605, anti-IgA (1040-08, Southern Biotech) biotin, anti-BAFF-R (8A7, eBioscience) PE, anti-CD21 (PB-306-T025, LT21, EXBIO) Pacific blue, anti-IgM (555783, G20-127, BD) PE, anti-IgD (9030-08, IADB6, Southern Biotech) biotin and anti-HLA-DR (559866, G46-6, BD) APC, and the levels of expression on the various B cell subsets, and the proportion of memory B cells expressing IgG or IgA were determined by gating on transitional, naive or memory B cells.

B and T cell cytokine profiling and in vitro differentiation

$CD4^+$ T cells were isolated as previously described42. PBMCs from healthy controls or SPPL2a- or IRF8-deficient patients were labeled with anti-CD4 APC-Cy7 (557871, RPA-T4, BD Biosciences), anti-CD45RA PerCpCy5.5 (45-0458-41, HI100, eBiosciences), anti-CCR7 FITC (MAB197-SP, 150503, R&D sytems), anti-CD25 PE (555432, M-A251, BD Biosciences) and anti-CD127 BV650 (351325, A019D5, BioLegend) Abs, and naive ($CD25^{lo}CD127^{hi}CD45RA^+CCR7^+CD4^+$) or memory ($CD25^{lo}CD127^{hi}CD45RA^-CCR7^{\pm}CD4^+$) T cells were isolated (> 98% purity) with a FACSAria (BD Biosciences). Purified memory $CD4^+$ T cells were cultured with T cell activation and expansion (TAE) beads (anti-CD2/CD3/CD28; Miltenyi Biotec) for 5 days. Purified naive $CD4^+$ T cells were cultured with TAE beads alone or under T_H1 (IL-12 [20 ng/ml; R&D Systems]), T_H2 (IL-4) or T_H17 (TGF-β, IL-1β [20 ng/ml; Peprotech], IL-6 [50 ng/mL; PeproTech], IL-21 [50 ng/mL; PeproTech], IL-23 [20 ng/mL; eBioscience], anti–IL-4 [5 μg/mL], and anti-IFN-γ [5 μg/mL; eBioscience]) polarizing conditions for 5 days. Supernatants were then harvested and their content of IL-2, IL-4, IL-5, IL-6, IL-9, IL-10, IL-13, IL-17A, IL-17F, IFN-γ and TNF was determined in cytometric bead arrays (BD Biosciences); IL-22 was determined by ELISA. For cytokine expression, activated $CD4^+$ T cells were restimulated with PMA (100 ng/ml)/ionomycin (750 ng/ml) for 6 hours, with the addition of brefeldin A (10 μg/ml) after 2 hours. Cells were then fixed and their intracellular cytokine profiles were determined.

B cell culture

PBMCs from healthy controls or SPPL2A-deficient patients were labeled with anti-CD20 Pe-Cy7 (25-0209-42, 2H7, eBioscience), anti-CD10 APC (340923, HI10a, BD Bioscience), and anti-CD27 Pe (555441, M-T271, BD Bioscience) Abs and naive ($CD20^+CD10^-CD27^-IgG^-$) and memory ($CD20^+CD10^-CD27^+$) B cells were purified by cell sorting (FACSAria, BD Biosciences). They were cultured in the presence of CD40L, either alone or together with IL-21. After eight days, culture supernatants were harvested and the secretion of IgM, IgG and IgA was determined by Ig heavy chain-specific ELISA59.

T cell library and T cell clone generation and measurement of cytokine production

Two subsets of $CD4^+CD45RA^-CD25^-CD19^-CD8^-$ memory T cells were sorted from total PBMCs, on the basis of CCR6 expression, with a FACS Aria (BD Biosciences), after the exclusion of $CD45RA^+CCR7^+$ naive T cells. The $CCR6^+$ subset, including T cells producing IL-17 and IFN-γ, and the $CCR6^-$ subset, including T cells producing IL-4 and IFN-γ, were collected44. The cells were cultured in RPMI 1640 medium supplemented with 2 mM glutamine, 1% (vol/vol) nonessential amino acids, 1% (vol/vol) sodium pyruvate, penicillin (50 U/ml), streptomycin (50 μg/ml) (all from Invitrogen) and 5% heat-inactivated human serum (Swiss RedCross). The sorted memory T cells (500 cells/well) were stimulated polyclonally with 1 μg/ml PHA (Remel) in the presence of irradiated (45 Gy) allogeneic feeder cells (2.5×10^4 per well) and IL-2 (500 IU/ml), in a 96-well plate, and cell lines were expanded, as previously described45. Library screening was performed 14-21 days after initial stimulation, by culturing thoroughly washed T cells ($2.5x10^5$/well) with autologous irradiated B cells ($2.5x10^4$), with or without a three-hour pulse of various antigens, including the CMV/EBV HLA class II peptide pool or the EBV HLA class II peptide pool (0.5 μg/ml/peptide, comprising 122 peptides (46 EBV and 76 CMV)), the MTB epitope pool (0.5 μg/ml/peptide, comprising 207 peptides), the BCG epitope pool (0.5 μg/ml/peptide, comprising 211 peptides), purified RSV A-2-containing lysate (100 μg/ml, Advanced Biotechnologies), influenza virus vaccine (Crucell) or *Candida albicans*-containing lysate (used at 5 μg/ml). Multiepitope peptide pools were prepared as previously described60. Proliferation was assessed on day 4, after incubation for 16 h with 1 μCi/ml [^{3}H]-thymidine (GE Healthcare). Precursor frequencies were calculated from the number of negative wells, assuming a Poisson distribution, and are expressed per million cells45. Cytokine concentrations in positive culture supernatants were determined after 48 hours of stimulation with cytometric bead arrays (BioLegend). T cell clones were made by sorting $ICOS^+CD25^+$ cells from antigen-stimulated T cell lines and plating them at 0.5 cells per well in 384 well plates in IL-2 complete media with 1 μg/ml PHA (Remel), and 50,000 irradiated allogenous PBMC per well. T cell clones were stained for FACS analysis and used in proliferation assays to assess antigen-presenting function of EBV-B cells from SPPL2A-deficient patient transduced with a retrovirus generated with a WT allele of *SPPL2A* or an empty vector gene as described avobe.

Mouse experiments

Flow cytometry—Mice (C57BL6/J) were killed and their spleens were removed and placed in cold RPMI supplemented with 3% FBS and 2% P/S. Single-cell suspensions were prepared and red blood cells were lysed in lysis buffer (155 mM NH_4Cl, 12 mM $NaHCO_3$, 0.1 mM EDTA). Cells were washed and plated at a density of 2×10^6 cells/well in a 96-well plate for cell staining in FACS buffer (PBS, 2% FBS). Viable cells were stained with Aqua Zombie Fixable Viability Dye (BioLegend) for 15 minutes at room temperature. Cells were surface-stained for 30 minutes at 4°C with the following Ab cocktail for DCs: anti-CD45 APC/eFluor 780 (47-0451-80, 30-F11, eBioscience), anti-CD11b PE-Cy7 (101215, M1/70, BioLegend), anti-CD11c PerCP/Cy5.5 (117327, N418, BioLegend), anti-CD8 eFluor (100707, 53-6.7, BioLegend), anti-CD49b PE (108907, DX5, BioLegend), anti-CD19 PE (152407, 1D3, BioLegend), anti-TCRβ PE (109207, H57-597, BioLegend), anti-Ly6G PE

(127607, 1A8, BioLegend), anti-TCRγδ PE (118107, GL3, BioLegend). Cells were fixed and sorted with an eight-color FACS Canto II machine equipped with FACS Diva software (BD Biosciences). The data obtained were analyzed with FlowJo software (Tree Star). In total, 10^5 cells were acquired and aggregates were removed on the basis of forward scatter height (FSC-H) vs. area (FSC-A). Debris removal was evaluated by assessing side scatter area (SSC-A) and FSC-A. Viable cells were identified by gating on the population negative for Aqua Zombie viability dye (V500), and leukocytes were isolated as $CD45^+$ cells. All Abs were obtained from eBioscience unless otherwise stated.

Analysis of cytokine production—For intracellular cytokine staining, spleen single-cell suspensions were plated in a 96-well plate at a density of $2x10^5$ cells in complete RPMI medium. Cells were incubated at 37°C for 6 hours with either 20 MOI of live *M. bovis* (BCG) or PMA (50 ng/mL) and ionomycin (500 ng/mL). Cells were washed and resuspended in FACS buffer for cell staining (as described above). Cells were surface-stained by incubation for 30 min at 4°C with the following Ab cocktail: anti-CD4 PerCP/Cy5.5 (100433, GK1.5, BioLegend), anti-CD8α eFluor 450 (48-0081080, 53-6.7, BioLegend). Cells were fixed and permeabilized and subjected to intracellular staining for 30 min at 4°C with the following Ab cocktail: anti-TNF APC (506307, MPG-XT22, BioLegend), anti-IFN-γ FITC (505805, XMG1.2, BioLegend), before analysis on a FACS Canto II instrument. All Abs were obtained from eBioscience unless otherwise stated. We determined cytokine levels in the culture supernatant of spleen cells, by plating cells in a 96-well plate at a density of $2x10^6$ cells in complete RPMI medium and stimulating them at 37°C for 48 hours with either 20 MOI of live *M. bovis* (BCG) or PMA (50 ng/ml) plus ionomycin (500 ng/ml). Cell supernatants were collected and cytokine levels were determined by ELISA (BioLegend).

Mycobacterium bovis (BCG) infection—Single-cell suspensions of *M. bovis* (BCG) were prepared for in vivo infection as previously described61. Briefly, $5x10^4$ colony-forming units (CFUs) were injected intravenously into 8- to 12-week-old WT and *Sppl2a*$^{-/-}$ mutant mice. Three or six weeks post-infection, mice were killed, weighed and the numbers of *M. bovis* BCG CFUs in the spleen were determined by homogenization and plating on Dubos oleic agar base, followed by three weeks of incubation at 37°C. Splenomegaly (spleen index), defined as the square root of spleen weight (x100) divided by body weight, was monitored.

MTB infection protocol—We infected 8- to 12-week-old mice with an aerosol of ~50 CFU of MTB H37Rv and monitored survival. Infectious dose was determined by the replication of colony-forming units (CFU) from total lung homogenates. In a separate experiment, we infected 8- to 12-week-old mice with an aerosol of ~50 CFU of MTB H37Rv and killed them 30 and 60 post-infection. Bacterial loads at these time points were determined by the replication of colony-forming units from lung homogenates. Immunophenotyping analysis was performed on the lungs, with single-cell suspensions generated by mechanical disruption and collagenase A digestion. Single cells from the lungs and spleen were processed as described above.

Animal ethics statement—For all mouse experiments, this study was performed in accordance and compliance with the guidelines and regulations of the Canadian Council on Animal Care (CCAC). All protocols were approved by the Animal Care Committee of McGill University. Mice were anesthetized, and euthanized by carbon dioxide inhalation, and every effort was made to minimize animal suffering.

ChIP-seq and RNA-seq

ChIP-seq datasets for transcription factors and epigenetic modifications in basal and stimulus-activated mouse primary macrophages were obtained from recent publications for: control IgG, IRF8, IRF1, PU.1, H3K4me1 and H3K27Ac62; STAT163; STAT264; p65 (NFκB)65; IRF5 66; CEBPα67; and RNA Pol II and H3K4me3 68. Sequence read density profiles (bigwig) were generated with the Homer tool and normalized to counts per 10^7 reads69. Gene expression profiles (RNA-seq) for primary mouse macrophages with and without IFN-γ treatment for 3 h are scaled per million reads and mapped onto the mm9 reference genome assembly62. The Integrative Genomics Viewer was used to visualize sequence read density profiles and to extract the genome browser snapshot for Fig. S7a70.

Supplementary Material

Refer to Web version on PubMed Central for supplementary material.

Acknowledgments

We thank B. Coller, C. Rice, X. Ma, M. Ciancanelli and G. Vogt for helpful discussions and critical reading. We thank Y. Nemirovskaya, E. Anderson, T. Kochetkov, M. Romanick, L. Amar, C. Patissier, C. Desvallées, M. Woollett, A. Gall and J. Gonzalez for technical and secretarial assistance and all members of the Laboratory of Human Genetics of Infectious Diseases for helpful discussions. We thank F. Batteux and M. Bahuad from the Laboratory of Immunology, Cochin Hospital, Paris-France for serological testing patients and F. B. Menozzi and the Microbiology Institute, EOC, Bellinzona for providing microbial products. X-F.K. was supported by the Jerome Lejeune Foundation, the Stony Wold-Herbert Fund, the Choh-Hao Li Memorial Fund Scholar Award and the Shanghai Educational Development Foundation. R.M.B. was funded by a European Molecular Biology Organization (EMBO) long-term fellowship. J.M. was supported by the Charles H. Revson Senior Fellowship in Biomedical Sciences. B.S. received support from the *Deutsche Forschungsgemeinschaft* as part of the SFB877 and the Cluster of Excellence “Inflammation at Interfaces”, and the SCHR 1284/1-1 grant. The Laboratory of Human Genetics of Infectious Diseases is supported by grants from the St. Giles Foundation, the Jeffrey Modell Foundation, The Rockefeller University Center for Clinical and Translational Science grant number 8UL1TR000043 from the National Center for Research Resources and the National Center for Advancing Sciences (NCATS), the National Institutes of Health, the National Institute of Allergy and Infectious Diseases (5R01AI089970-02 and 5R37AI095983), grants from the Integrative Biology of Emerging Infectious Diseases Laboratory of Excellence (ANR-10-LABX-62-IBEID) and the French National Research Agency (ANR) under the “Investments for the future” program (ANR-10-IAHU-01), ANR-IFNGPHOX (ANR-13-ISV3-0001-01, to J.B.) and ANR-GENMSMD (ANR-16-CE17-0005-01, to J.B.), *Institut National de la Santé et de la Recherche Médicale* (INSERM), Paris Descartes University and The Rockefeller University. E.K.D., C.S.M. and S.G.T. are supported by research grants and fellowships from the National Health and Medical Research Council of Australia. DL was supported by a fellowship from the *Fonds de Recherche du Québec Santé*. Work in the P.G. laboratory was supported by a grant from the National Institute of Allergy and Infectious Diseases (R01AI035237-19). The work at the Institute for Research in Biomedicine is supported by grants from the ERC (323183 PREDICT, to F.S.), the Swiss National Science Foundation (170213 to F.S.) and the Helmut Horten Foundation. This work was supported by Award U19AI118626, NIH NIAID (to A.S. and F.S.).

References

1. Bustamante J, et al. Mendelian susceptibility to mycobacterial disease: Genetic, immunological, and clinical features of inborn errors of IFN-gamma immunity. Semin Immunol. 2014; 26:454–470. [PubMed: 25453225]

2. Casanova JL, Abel L. Genetic dissection of immunity to mycobacteria: the human model. Annu Rev Immunol. 2002; 20:581–620. [PubMed: 11861613]

3. de Beaucoudrey L, et al. Revisiting human IL-12Rbeta1 deficiency: a survey of 141 patients from 30 countries. Medicine. 2010; 89:381–402. [PubMed: 21057261]

4. Dupuis S, et al. Human interferon-gamma-mediated immunity is a genetically controlled continuous trait that determines the outcome of mycobacterial invasion. Immunol Rev. 2000; 178:129–137. [PubMed: 11213797]

5. Kreins AY, et al. Human TYK2 deficiency: Mycobacterial and viral infections without hyper-IgE syndrome. The Journal of experimental medicine. 2015; 212:1641–1662. [PubMed: 26304966]

6. Bogunovic D, et al. Mycobacterial disease and impaired IFN-gamma immunity in humans with inherited ISG15 deficiency. Science. 2012; 337:1684–1688. [PubMed: 22859821]

7. Bustamante J, et al. Germline CYBB mutations that selectively affect macrophages in kindreds with X-linked predisposition to tuberculous mycobacterial disease. Nat Immunol. 2011; 12:213–221. [PubMed: 21278736]

8. Boisson-Dupuis S, et al. Inherited and acquired immunodeficiencies underlying tuberculosis in childhood. Immunol Rev. 2015; 264:103–120. [PubMed: 25703555]

9. Nathan CF, et al. Identification of interferon-gamma as the lymphokine that activates human macrophage oxidative metabolism and antimicrobial activity. The Journal of experimental medicine. 1983; 158:670–689. [PubMed: 6411853]

10. Prando C, et al. Inherited IL-12p40 deficiency: genetic, immunologic, and clinical features of 49 patients from 30 kindreds. Medicine. 2013; 92:109–122. [PubMed: 23429356]

11. Kong XF, et al. A novel homozygous p.R1105X mutation of the AP4E1 gene in twins with hereditary spastic paraplegia and mycobacterial disease. PLoS One. 2013; 8:e58286. [PubMed: 23472171]

12. Itan Y, et al. The mutation significance cutoff: gene-level thresholds for variant predictions. Nature methods. 2016; 13:109–110. [PubMed: 26820543]

13. Voss M, et al. Mechanism, specificity, and physiology of signal peptide peptidase (SPP) and SPP-like proteases. Biochim Biophys Acta. 2013; 1828:2828–2839. [PubMed: 24099004]

14. Brady OA, et al. Regulated intramembrane proteolysis of the frontotemporal lobar degeneration risk factor, TMEM106B, by signal peptide peptidase-like 2a (SPPL2a). J Biol Chem. 2014; 289:19670–19680. [PubMed: 24872421]

15. Fluhrer R, et al. A gamma-secretase-like intramembrane cleavage of TNFalpha by the GxGD aspartyl protease SPPL2b. Nat Cell Biol. 2006; 8:894–896. [PubMed: 16829951]

16. Friedmann E, et al. SPPL2a and SPPL2b promote intramembrane proteolysis of TNFalpha in activated dendritic cells to trigger IL-12 production. Nature cell biology. 2006; 8:843–848. [PubMed: 16829952]

17. Kirkin V, et al. The Fas ligand intracellular domain is released by ADAM10 and SPPL2a cleavage in T-cells. Cell Death Differ. 2007; 14:1678–1687. [PubMed: 17557115]

18. Martin L, et al. Regulated intramembrane proteolysis of Bri2 (Itm2b) by ADAM10 and SPPL2a/SPPL2b. J Biol Chem. 2008; 283:1644–1652. [PubMed: 17965014]

19. Beisner DR, et al. The intramembrane protease Sppl2a is required for B cell and DC development and survival via cleavage of the invariant chain. The Journal of experimental medicine. 2013; 210:23–30. [PubMed: 23267013]

20. Bergmann H, et al. B cell survival, surface BCR and BAFFR expression, CD74 metabolism, and CD8- dendritic cells require the intramembrane endopeptidase SPPL2A. The Journal of experimental medicine. 2013; 210:31–40. [PubMed: 23267016]

21. Schneppenheim J, et al. The intramembrane protease SPPL2a promotes B cell development and controls endosomal traffic by cleavage of the invariant chain. The Journal of experimental medicine. 2013; 210:41–58. [PubMed: 23267015]

22. Fleck D, et al. Proteolytic Processing of Neuregulin 1 Type III by Three Intramembrane-cleaving Proteases. J Biol Chem. 2016; 291:318–333. [PubMed: 26574544]

23. Itan Y, et al. The human gene connectome as a map of short cuts for morbid allele discovery. Proceedings of the National Academy of Sciences of the United States of America. 2013; 110:5558–5563. [PubMed: 23509278]

24. Zhang Y, et al. Genomics is rapidly advancing precision medicine for immunological disorders. Nat Immunol. 2015; 16:1001–1004. [PubMed: 26382860]
25. Rieux-Laucat F. Inherited and acquired death receptor defects in human Autoimmune Lymphoproliferative Syndrome. Current directions in autoimmunity. 2006; 9:18–36. [PubMed: 16394653]
26. Ai JW, et al. The Risk of Tuberculosis in Patients with Rheumatoid Arthritis Treated with Tumor Necrosis Factor-alpha Antagonist: A Metaanalysis of Both Randomized Controlled Trials and Registry/Cohort Studies. The Journal of rheumatology. 2015; 42:2229–2237. [PubMed: 26472414]
27. Moreno-De-Luca A, et al. Adaptor protein complex-4 (AP-4) deficiency causes a novel autosomal recessive cerebral palsy syndrome with microcephaly and intellectual disability. Journal of medical genetics. 2011; 48:141–144. [PubMed: 20972249]
28. Schneppenheim J, et al. Signal-peptide-peptidase-like 2a is required for CD74 intramembrane proteolysis in human B cells. Biochemical and biophysical research communications. 2014; 451:48–53. [PubMed: 25035924]
29. Becker-Herman S, et al. CD74 is a member of the regulated intramembrane proteolysis-processed protein family. Mol Biol Cell. 2005; 16:5061–5069. [PubMed: 16107560]
30. Hambleton S, et al. IRF8 mutations and human dendritic-cell immunodeficiency. N Engl J Med. 2011; 365:127–138. [PubMed: 21524210]
31. Bridgeford EC, et al. Agammaglobulinemia and Staphylococcus aureus botryomycosis in a cohort of related sentinel Swiss Webster mice. Journal of clinical microbiology. 2008; 46:1881–1884. [PubMed: 18322060]
32. Conley ME, et al. Primary B cell immunodeficiencies: comparisons and contrasts. Annu Rev Immunol. 2009; 27:199–227. [PubMed: 19302039]
33. Reynolds G, Haniffa M. Human and Mouse Mononuclear Phagocyte Networks: A Tale of Two Species? Front Immunol. 2015; 6:330. [PubMed: 26124761]
34. Merad M, et al. The dendritic cell lineage: ontogeny and function of dendritic cells and their subsets in the steady state and the inflamed setting. Annu Rev Immunol. 2013; 31:563–604. [PubMed: 23516985]
35. Iwakoshi NN, et al. The transcription factor XBP-1 is essential for the development and survival of dendritic cells. The Journal of experimental medicine. 2007; 204:2267–2275. [PubMed: 17875675]
36. Dickinson RE, et al. The evolution of cellular deficiency in GATA2 mutation. Blood. 2014; 123:863–874. [PubMed: 24345756]
37. Bigley V, et al. Dendritic cell analysis in primary immunodeficiency. Curr Opin Allergy Clin Immunol. 2016; 16:530–540. [PubMed: 27755182]
38. Vignali DA, Kuchroo VK. IL-12 family cytokines: immunological playmakers. Nat Immunol. 2012; 13:722–728. [PubMed: 22814351]
39. See P, et al. Mapping the human DC lineage through the integration of high-dimensional techniques. Science. 2017; 356
40. Villani AC, et al. Single-cell RNA-seq reveals new types of human blood dendritic cells, monocytes, and progenitors. Science. 2017; 356
41. Breton G, et al. Circulating precursors of human CD1c+ and CD141+ dendritic cells. The Journal of experimental medicine. 2015; 212:401–413. [PubMed: 25687281]
42. Ma CS, et al. Unique and shared signaling pathways cooperate to regulate the differentiation of human CD4+ T cells into distinct effector subsets. The Journal of experimental medicine. 2016; 213:1589–1608. [PubMed: 27401342]
43. Teng MW, et al. IL-12 and IL-23 cytokines: from discovery to targeted therapies for immune-mediated inflammatory diseases. Nature medicine. 2015; 21:719–729.
44. Acosta-Rodriguez EV, et al. Surface phenotype and antigenic specificity of human interleukin 17-producing T helper memory cells. Nature immunology. 2007; 8:639–646. [PubMed: 17486092]
45. Geiger R, et al. Human naive and memory CD4+ T cell repertoires specific for naturally processed antigens analyzed using libraries of amplified T cells. The Journal of experimental medicine. 2009; 206:1525–1534. [PubMed: 19564353]

46. Marquis JF, et al. Interferon regulatory factor 8 regulates pathways for antigen presentation in myeloid cells and during tuberculosis. PLoS Genet. 2011; 7:e1002097. [PubMed: 21731497]
47. Berghout J, et al. Irf8-regulated genomic responses drive pathological inflammation during cerebral malaria. PLoS Pathog. 2013; 9:e1003491. [PubMed: 23853600]
48. Bigley V, et al. The human syndrome of dendritic cell, monocyte, B and NK lymphoid deficiency. The Journal of experimental medicine. 2011; 208:227–234. [PubMed: 21242295]
49. Kindler V, et al. The inducing role of tumor necrosis factor in the development of bactericidal granulomas during BCG infection. Cell. 1989; 56:731–740. [PubMed: 2647299]
50. Keane J, et al. Tuberculosis associated with infliximab, a tumor necrosis factor alpha-neutralizing agent. N Engl J Med. 2001; 345:1098–1104. [PubMed: 11596589]
51. Martínez-Barricarte R, et al. Transduction of Herpesvirus saimiri-Transformed T Cells with Exogenous Genes of Interest. Curr Protoc Immunol. 2016; 115:7.21C.21–27.21C.12. [PubMed: 27801513]
52. Schneppenheim J, et al. The intramembrane proteases signal Peptide peptidase-like 2a and 2b have distinct functions in vivo. Mol Cell Biol. 2014; 34:1398–1411. [PubMed: 24492962]
53. Li H, Durbin R. Fast and accurate short read alignment with Burrows-Wheeler transform. Bioinformatics. 2009; 25:1754–1760. [PubMed: 19451168]
54. McKenna A, et al. The Genome Analysis Toolkit: a MapReduce framework for analyzing next-generation DNA sequencing data. Genome research. 2010; 20:1297–1303. [PubMed: 20644199]
55. Wang K, et al. ANNOVAR: functional annotation of genetic variants from high-throughput sequencing data. Nucleic acids research. 2010; 38:e164. [PubMed: 20601685]
56. Purcell S, et al. PLINK: a tool set for whole-genome association and population-based linkage analyses. American journal of human genetics. 2007; 81:559–575. [PubMed: 17701901]
57. Abecasis GR, et al. Merlin--rapid analysis of dense genetic maps using sparse gene flow trees. Nature genetics. 2002; 30:97–101. [PubMed: 11731797]
58. Breton G, et al. Defining human dendritic cell progenitors by multiparametric flow cytometry. Nature protocols. 2015; 10:1407–1422. [PubMed: 26292072]
59. Avery DT, et al. B cell-intrinsic signaling through IL-21 receptor and STAT3 is required for establishing long-lived antibody responses in humans. The Journal of experimental medicine. 2010; 207:155–171. [PubMed: 20048285]
60. Lindestam Arlehamn CS, et al. A Quantitative Analysis of Complexity of Human Pathogen-Specific CD4 T Cell Responses in Healthy M. tuberculosis Infected South Africans. PLoS Pathog. 2016; 12:e1005760. [PubMed: 27409590]
61. Gros P, et al. Genetic control of natural resistance to Mycobacterium bovis (BCG) in mice. Journal of immunology. 1981; 127:2417–2421.
62. Langlais D, et al. The macrophage IRF8/IRF1 regulome is required for protection against infections and is associated with chronic inflammation. The Journal of experimental medicine. 2016; 213:585–603. [PubMed: 27001747]
63. Ng SL, et al. IκB kinase epsilon (IKK(epsilon)) regulates the balance between type I and type II interferon responses. Proceedings of the National Academy of Sciences of the United States of America. 2011; 108:21170–21175. [PubMed: 22171011]
64. Mancino A, et al. A dual cis-regulatory code links IRF8 to constitutive and inducible gene expression in macrophages. Genes & development. 2015; 29:394–408. [PubMed: 25637355]
65. Barish GD, et al. Bcl-6 and NF-kappaB cistromes mediate opposing regulation of the innate immune response. Genes & development. 2010; 24:2760–2765. [PubMed: 21106671]
66. Saliba DG, et al. IRF5:RelA interaction targets inflammatory genes in macrophages. Cell reports. 2014; 8:1308–1317. [PubMed: 25159141]
67. Kaikkonen MU, et al. Remodeling of the enhancer landscape during macrophage activation is coupled to enhancer transcription. Mol Cell. 2013; 51:310–325. [PubMed: 23932714]
68. Ostuni R, et al. Latent enhancers activated by stimulation in differentiated cells. Cell. 2013; 152:157–171. [PubMed: 23332752]

69. Heinz S, et al. Simple combinations of lineage-determining transcription factors prime cis-regulatory elements required for macrophage and B cell identities. Mol Cell. 2010; 38:576–589. [PubMed: 20513432]

70. Thorvaldsdottir H, et al. Integrative Genomics Viewer (IGV): high-performance genomics data visualization and exploration. Briefings in bioinformatics. 2013; 14:178–192. [PubMed: 22517427]

Europe PMC Funders Author Manuscripts

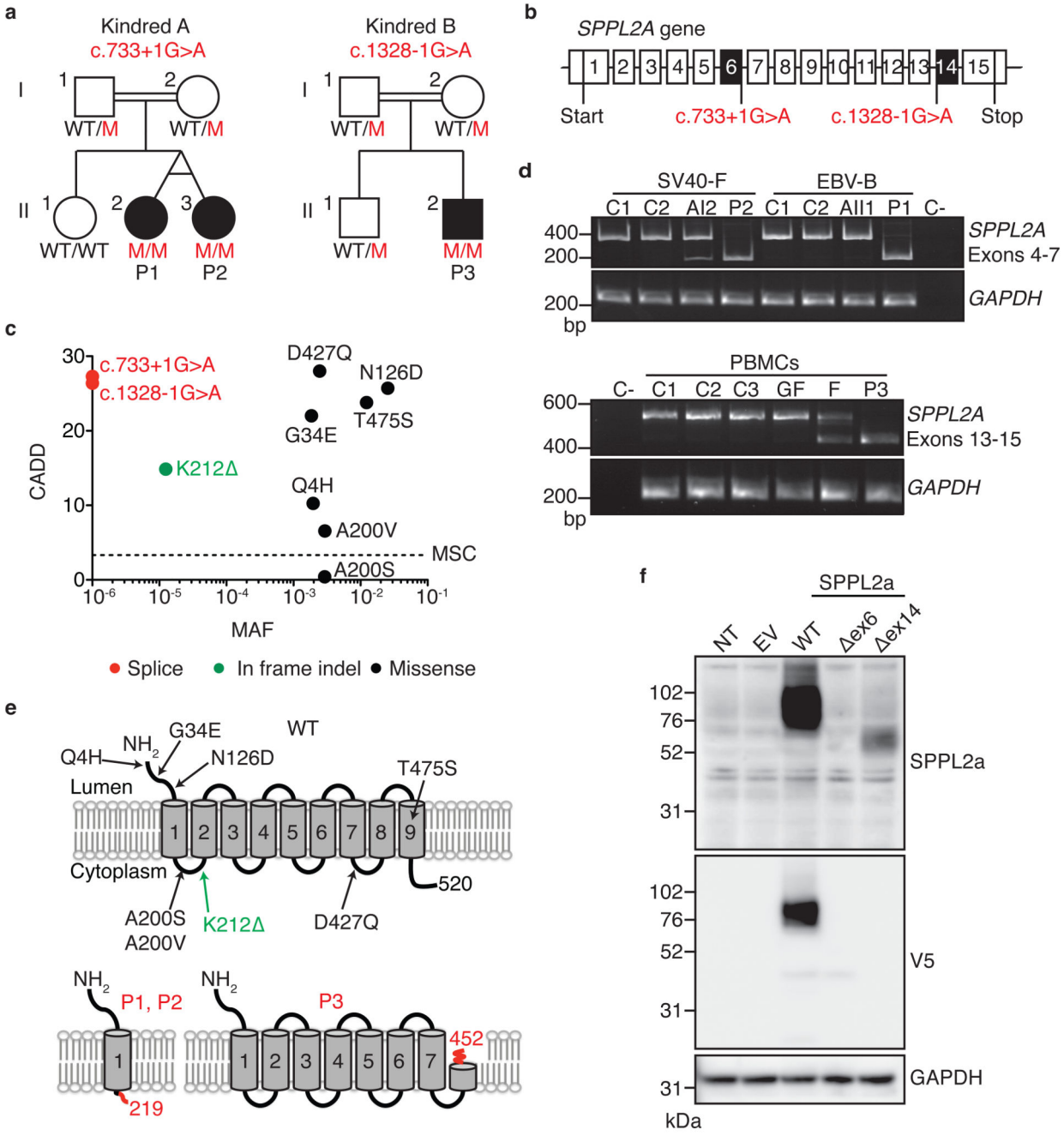

Figure 1. Discovery and in vitro characterization of *SPPL2A* mutations.

a) Pedigrees and familial segregation of the two mutations are shown. In red, M denotes the mutation in each family as indicated above each pedigree. Solid symbols indicate affected individuals. **b)** Schematic representation of the *SPPL2A* gene. Each numbered box represents an exon. The mutations studied here are marked in red. Black exons were spliced out due to the mutations. **c)** CADD score (*y*-axis) against minor allele frequency (MAF, *x*-axis) for the mutations found in our patients and homozygous variations described in the gnomAD database. **d)** PCR of exons 4 to 7 and 13 to 15 of *SPPL2A* cDNA from SV40-

Europe PMC Funders Author Manuscripts

Fibroblasts, EBV-B cells and PBMC from healthy controls, the three patients and their relatives. GF is the paternal grandfather (WT/WT) and F is the father (WT/M) from kindred B. Results shown are representative of two independent experiments. **e)** Schematic representation of the structure of WT SPPL2a in which the variants from Fig. 1c are indicated. The schemes in the lower part of the figure show the predicted consequences of the mutations. Each mutation causes a frameshift leading to a predicted non-canonical sequence indicated in red and a premature stop codon, at positions 219 and 452, respectively. **f)** Immunoblot analysis of SPPL2a in HEK293T cells left non-transfected (NT) or transfected with an empty vector (EV), WT *SPPL2A*, *SPPL2AΔex6* or *SPPL2AΔex14,* all C-terminally V5 tagged. Two Abs were used: an N-terminal anti-SPPL2a and an anti-V5 tag. GAPDH served as a protein loading control. Results shown are representative of three independent experiments.

Europe PMC Funders Author Manuscripts

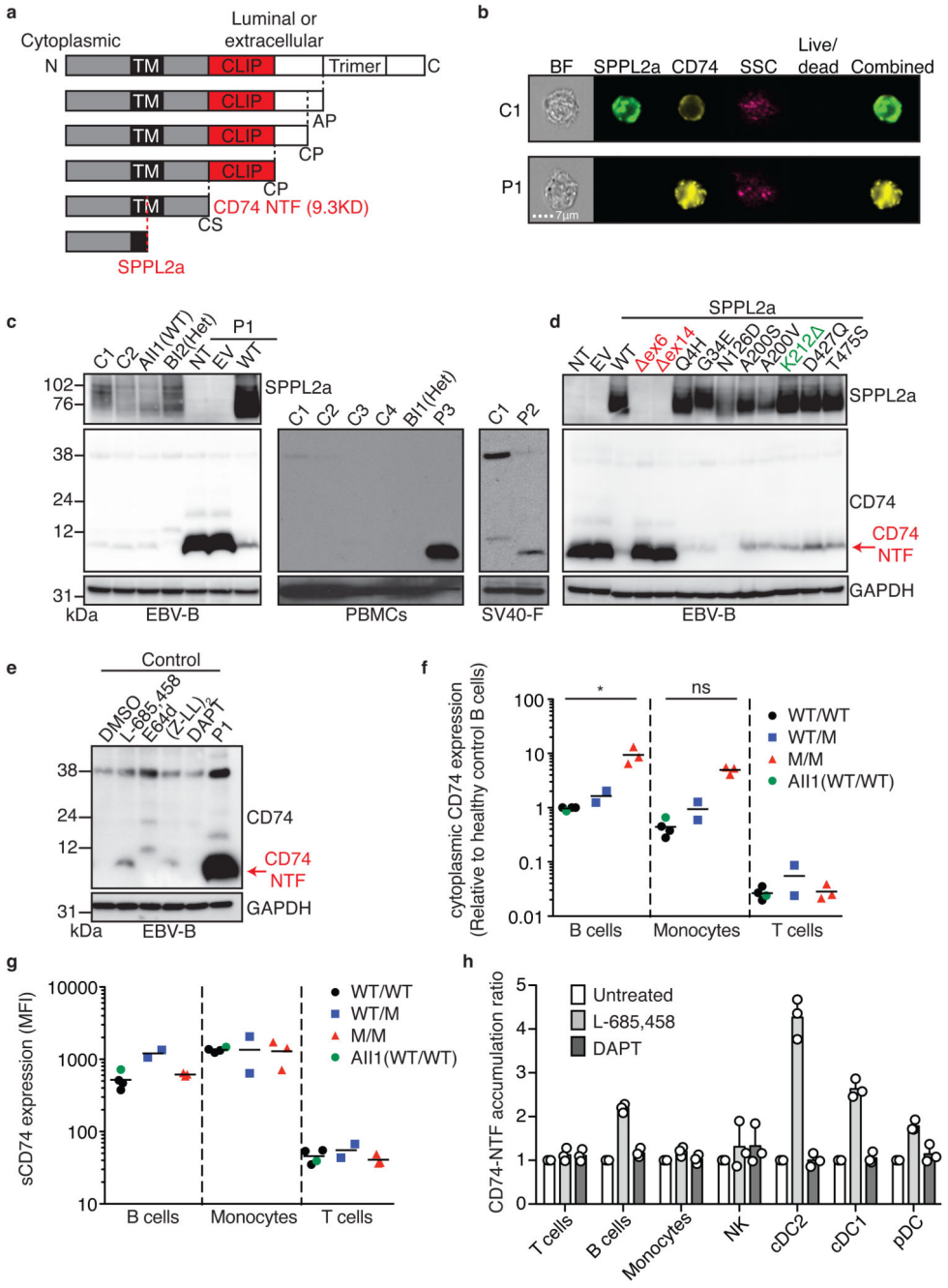

Figure 2. A lack of SPPL2a function leads to the accumulation of CD74 NTF.

a) Schematic representation of CD74 proteolytic processing by aspartic proteases (AP), cysteine proteases (CP), cathepsin S (CS) and SPPL2a. **b)** Imagestream analysis of EBV-B cells from P1 and a healthy control (C1). Intracellular staining for SPPL2a and CD74 individually or combined, SSC, bright field (BF) and live/dead marker are shown. **c)** Immunoblot analysis of SPPL2a and CD74 of EBV-B cells from P1, either non-transduced (NT), transduced with a retrovirus produced with an empty vector (EV) or a WT *SPPL2A* allele, IFN-γ-stimulated SV40-Fibroblasts from P2 and PBMCs from P3 and appropriate

Europe PMC Funders Author Manuscripts

controls. GAPDH served as a loading control. **d)** Immunoblot analysis of SPPL2a and CD74 of EBV-B cells from P1, NT, EV, transduced with a retrovirus containing a WT *SPPL2A* allele, or the variants shown in Fig. 1c. GAPDH served as a loading control. **e)** Immunoblot analysis of CD74 in healthy control EBV-B cells treated with DMSO, L-685,458, DAPT, $(Z\text{-}LL)_2$, or (E64d) and P1 EBV-B cells. GAPDH served as a loading control. **f)** Intracellular CD74 levels in monocytes, B and T cells from P1-P3 and controls normalized against the MFI of the CD74 signal in B cells from healthy controls. *t*-test with a 95% confidence was used (* $p<0.05$). **g)** MFI of cell-surface CD74 expression for the same samples as in Fig. 2f. **h)** Intracellular CD74 staining of different immune cell subsets with and without L-685,458 or DAPT treatment. (b-e and h were each tested twice with identical results. f and g were done once. Graphs show mean and S.D.).

Europe PMC Funders Author Manuscripts

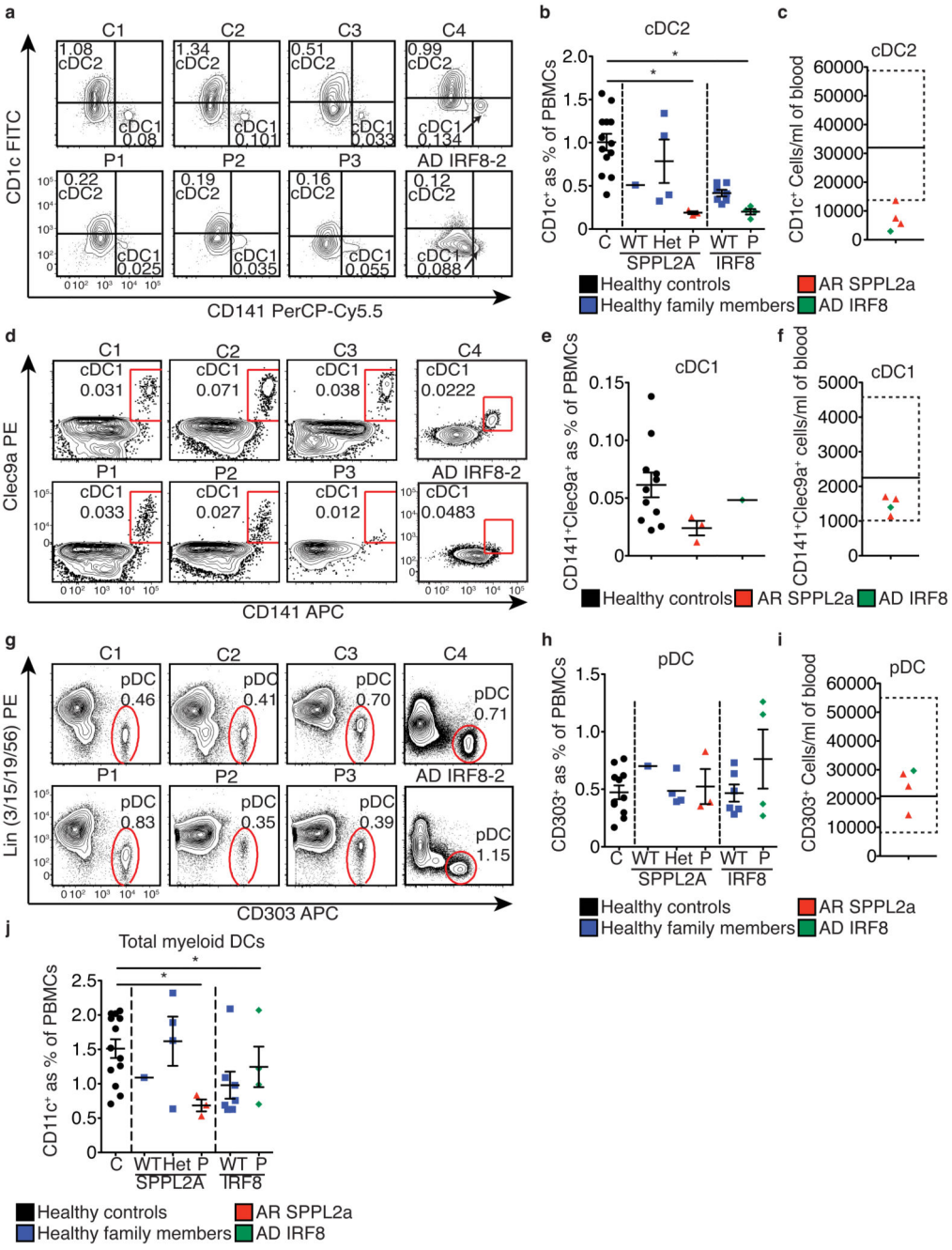

Figure 3. Mature dendritic cell immunophenotyping.

The frequencies of three subsets of circulating DCs were assessed in healthy controls, AR SPPL2a deficient patients, AD IRF8 deficient patients and family members. FACS plots coming from Fig. S4a, quantification as % of PBMCs and as cells per ml showing the normal range values from Thiant *et al.* (2017) as a dashed square are shown for **a-c)** cDC2, **d-f)** cDC1 and **g-i)** pDC. **j)** Total frequency of myeloid DCs.

The two AD IRF8 deficient patients were immunophenotyped twice for b, h and j but only individual values were used for statistical analysis. An unpaired two-tailed *t*-test with a 95%

confidence interval was used (* $p<0.05$). Non-significant results are not shown. All graphs show the mean with or without S.E.M. All these experiments were performed twice with identical results with the exception of cDC1 immunophenotyping for AR IRF8 deficient patient for d, e and f which was performed once.

Europe PMC Funders Author Manuscripts

Europe PMC Funders Author Manuscripts

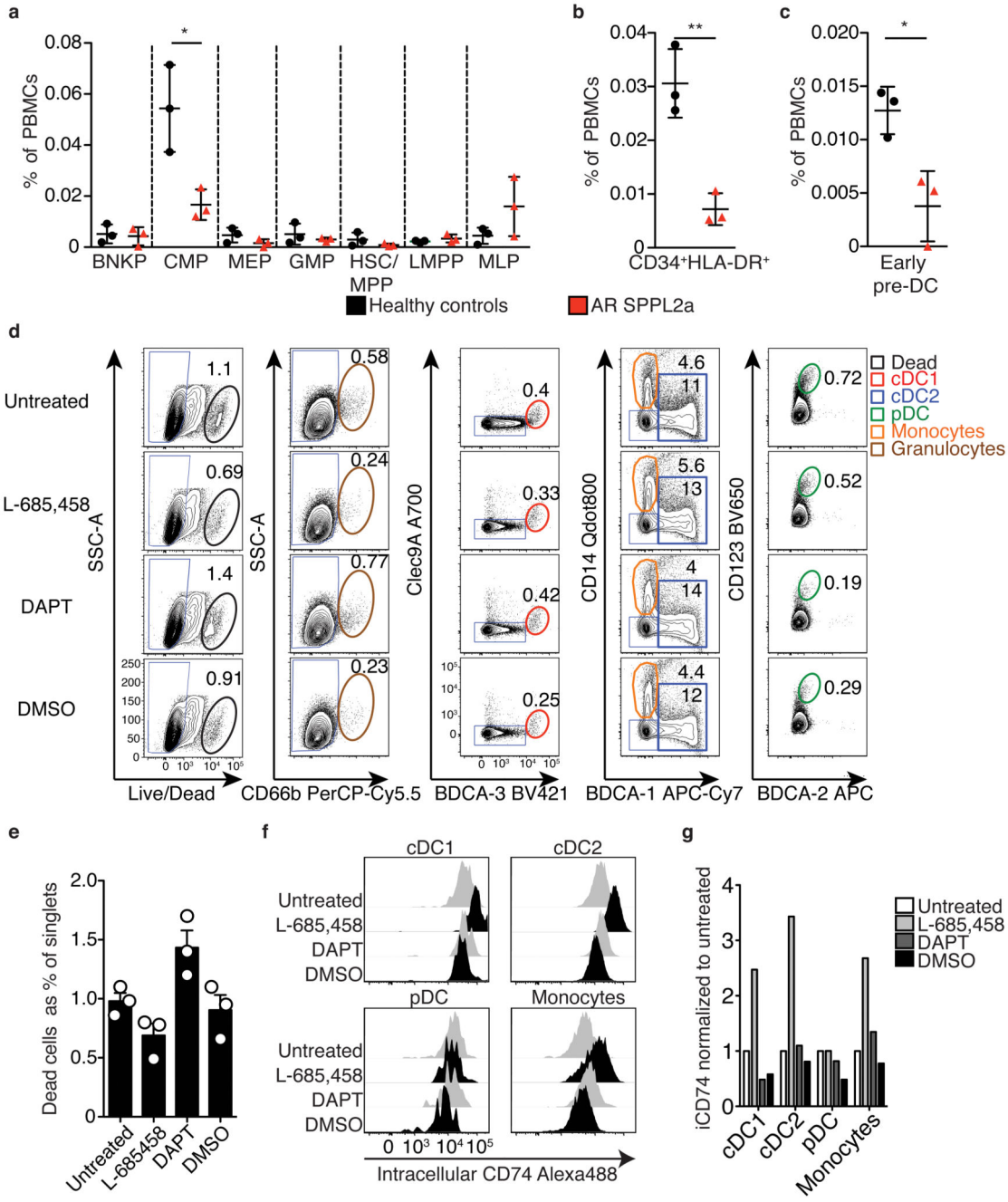

Figure 4. Progenitor DC immunophenotyping and DC *in vitro* differentiation.

a) Frequencies of BNKP, CMP, MEP, GMP, HSC/MPP, LMPP and MLP progenitors in healthy controls and SPPL2a-deficient patients. Gating in Fig. S5a,b. **b)** Frequency of $CD34^{+}HLA\text{-}DR^{+}$ progenitors in healthy controls and SPPL2a-deficient patients. Gating in Fig. S4d. **c)** Frequency of early pre-DCs in healthy controls and SPPL2a-deficient patients. Gating is shown in Fig. S4f. **d)** Differentiation potential of GMDPs in MS-5 stromal cells + cytokines cultured with or without SPPL2a inhibitor (L-685,458), DAPT or DMSO. **e)** Percentage of dead cells, for single $CD45^{+}$ cells either untreated or treated with L-685,458,

DAPT or DMSO. **f)** Intracellular CD74 levels incDC1s, cDC2s, pDCs and monocytes, after the in vitro differentiation from GMDPs, with or without L-685,458, DAPT or DMSO. **g)** MFI for intracellular CD74 from (f) normalized against the values of the untreated samples to show fold-accumulation.

An unpaired two-tailed *t*-test with a 95% confidence interval was used (* $p<0.05$, ** $p<0.01$). Non-significant results are not shown. All graphs show the mean with or without S.D. Immunophenotyping for a-c was done once. d, f and g show the representative results of one out of three experiments.

Europe PMC Funders Author Manuscripts

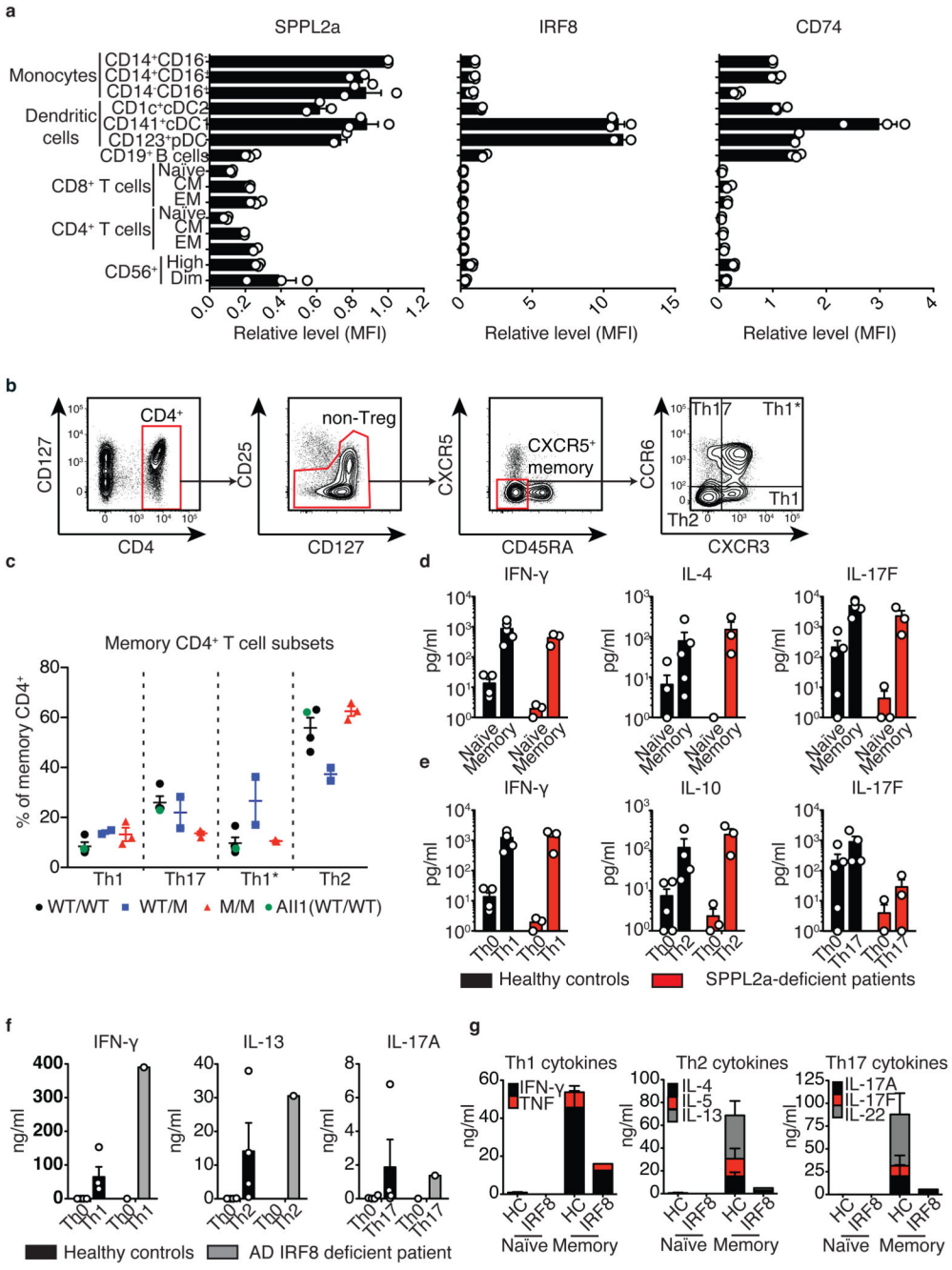

Figure 5. SPPL2a, IRF8 and CD74 profiling in leukocytes and CD4$^+$ T cell studies in patients with AR SPPL2a and AD IRF8 deficiencies.

a) Expression of SPPL2a, IRF8 and CD74 in the various subsets indicated on the *y*-axis. MFI was normalized against the levels of expression in CD14$^+$CD16$^-$ monocytes. **b)** Example of the gating strategy used for (c). **c)** Frequencies of four populations of CD4$^+$ memory T cells: Th1 (CCR6$^-$CCR4$^-$CXCR3$^+$), Th1* (CCR6$^+$CCR4$^-$CXCR3$^+$), Th17 (CCR6$^+$CCR4$^+$CXCR3$^-$) and Th2 (CCR6$^-$CCR4$^+$CXCR3$^-$). **d)** Naïve and memory CD4$^+$ T cells from healthy controls and patients with AR SPPL2a deficiency were stimulated with

TAE beads and the production of IFN-γ, IL-4 and IL-17F was measured after five days. **e)** Naïve $CD4^+$ T cells from healthy controls and patients with AR SPPL2a deficiency were cultured with TAE beads, alone or under Th1, Th2 or Th17 polarizing conditions. IFN-γ, IL-10 and IL-17F levels were determined in the corresponding polarizing conditions 5 days later. **f)** Naïve $CD4^+$ T cells from healthy controls and a patient with AD IRF8 deficiency were cultured with TAE beads, alone or under Th1, Th2 or Th17 polarizing conditions. IFN-γ, IL-13 and IL-17A levels were determined in the corresponding polarizing conditions 5 days later. **g)** Naïve and memory $CD4^+$ T cells from healthy controls and patients with AR SPPL2a deficiency were stimulated with TAE beads and the production of Th1 cytokines (IFN-γ and TNF), Th2 cytokines (IL-4, IL-5 and IL-13) and Th17 cytokines (IL-17A/F and IL-22) was measured after 5 days. The graphs in this figure show the mean and S.E.M.

Europe PMC Funders Author Manuscripts

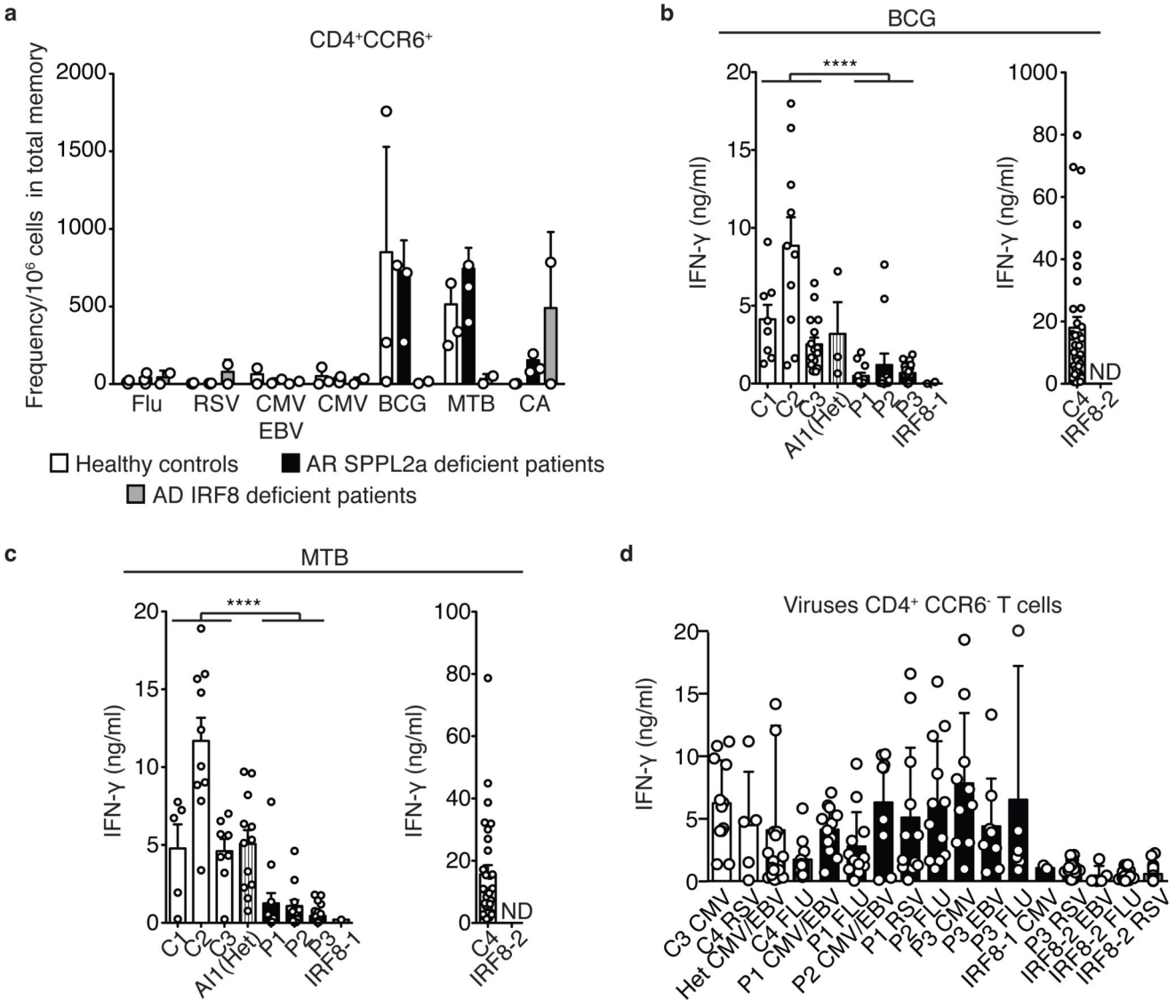

Figure 6. BCG and MTB-specific CD4$^+$CCR6$^+$ T cells from SPPL2a-mutant individuals display impaired IFN-γ production.

a) Frequency of CD4$^+$ T cells reactive with the indicated antigens in the CCR6$^+$ memory subsets (comprising T_H17 and T_H1* cells) from controls, patients with AR SPPL2a deficiency and patients with AD IRF8 deficiency. **b)** IFN-γ production by BCG-specific or **c)** MTB-specific CD4$^+$ T cells from the CCR6$^+$ memory subsets. ND indicates non-determined, due to the absence of cell lines proliferating in response to these stimuli. **d)** IFN-γ production by virus-specific CD4$^+$CCR6$^-$ cell lines from healthy controls, and patients with AR SPPL2a deficiency or AD IRF8 deficiency. The virus assessed and the individual from which the sample was obtained are indicated under each bar. The *p* values observed in this figure correspond to an unpaired two-tailed *t*-test with a 95% confidence interval (**** $p<0.0001$). Non-significant results are not shown. All graphs show mean and S.E.M.

Europe PMC Funders Author Manuscripts

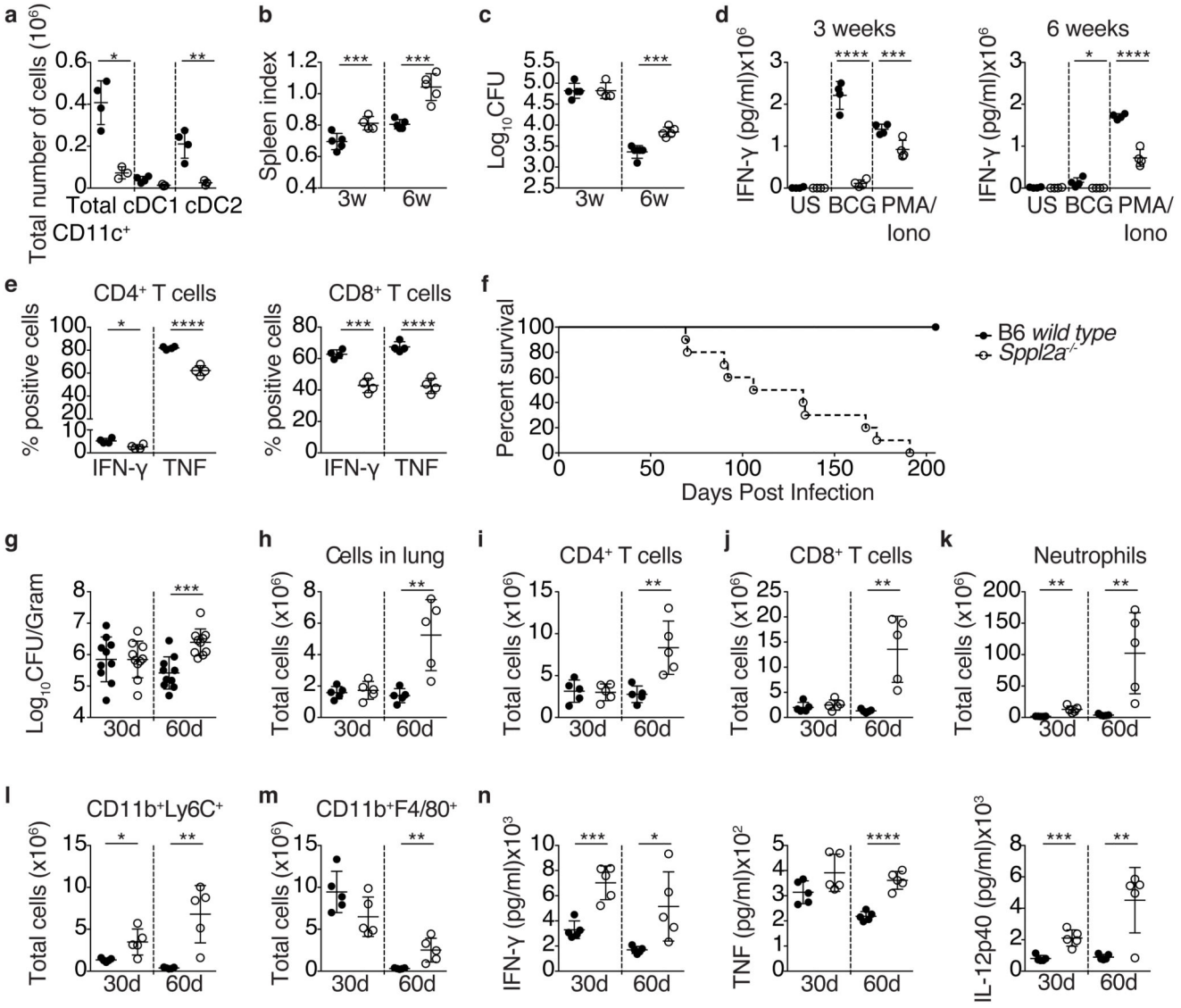

Figure 7. Sppl2a deficiency causes DC deficiencies and a predisposition to mycobacterial infection in mice.

a) Frequencies of $CD11c^+CD8^+$ (cDC1) and $CD11c^+CD11b^+$ (cDC2) dendritic cells in non-infected B6 WT and *Sppl2a*$^{-/-}$ mice, measured as a total number of cells. **b)** Spleen index and **c)** BCG CFU count of B6 WT and *sppl2a*$^{-/-}$ mice 3 and 6 weeks after BCG infection. **d)** Measurement of supernatant IFN-γ levels 3 and 6 weeks after infection. **e)** Percentages of IFN-γ^+ and TNF^+ CD4 and CD8 T cells in *Sppl2a*$^{-/-}$ mice. **f)** Survival curve of *Sppl2a*$^{-/-}$ and B6 WT mice infected with a MTB aerosol. **g)** MTB CFU counts of B6 WT and *sppl2a*$^{-/-}$ mice 30 and 60 days after infection with MTB aerosol. Quantification, in the lung, at 30 and 60 days post MTB aerosol infection, of **h)** total immune cells, **i)** $CD4^+$ T cells, **j)** $CD8^+$ T cells, **k)** neutrophils, **l)** $CD11b^+Ly6C^+$ monocytes and **m)** $CD11b^+F4/80^+$ macrophages, represented as total cells. **n)** Production of IFN-γ, TNF and IL-12p40 by lung homogenates after re-stimulation with MTB at 30 and 60 days post-infection. The *p* values presented in this figure correspond to an unpaired two-tailed *t*-test with a 95% confidence

interval (* p<0.05, ** p<0.01, *** p<0.001, **** p<0.0001). Non-significant results are not shown. All graphs except f show mean and S.E.M.

Europe PMC Funders Author Manuscripts